**Final Technical Report**
***Award #: G10AP00028***

**Title**: Assessing FEMA HAZUS-MH MR3: Constraining seismic hazard estimates for Riverside County using precariously balanced rocks and seismic amplification data

**Author**: E. S. Cochran
900 University Ave
Department of Earth Sciences
University of California
Riverside, CA 92521

**Term**: January 1, 2010 – December 31, 2011 (including one year no cost extension)

**Abstract**:

HAZUS-MH MR4 (HAZards U. S. Multi-Hazard Maintenance Release 4) is a risk-estimation software developed by FEMA to estimate potential losses from natural disasters. Federal, state, regional, and local governments use the HAZUS Earthquake Model for earthquake risk mitigation, preparedness, response, and recovery planning. First, to better understand the benefits and limitations of HAZUS, we examine input parameters used by the HAZUS Earthquake Model methodology to understand how modifying the user-defined settings affect ground motion analysis, seismic risk assessment, and earthquake loss estimates. Inputs analyzed include: 1) source parameters for deterministic event scenarios and 2) geologic site conditions. HAZUS calculates ground motion and resulting ground failure to estimate direct physical damage for general building stock, essential facilities, and lifelines, including transportation systems and utility systems. Earthquake losses in HAZUS are expressed in structural, economic and social terms; here we focus on monetary structural damages. This analysis centers on both shallow crustal and deep intraslab events that affect King County, Washington in the Pacific Northwest. We find that source and site input modifies the estimated economic building damage between a factor of 3.3 and 566, with a median of 6.6 for the seven earthquakes modeled. In addition, our results suggest that HAZUS model outcomes are more sensitive to changes in source parameters than site conditions. Second, we estimate the accelerations needed to topple precariously balanced rocks located on the UC Riverside campus, located near the active San Jacinto and San Andreas faults. In preliminary results we find preliminary toppling accelerations between 3.96 $m/s^2$ and 10.93 $m/s^2$ (40-111% *g*) would be needed to topple three of the PBRs. We also examine local variations in site amplification at this rock site to ensure ground motions are fairly uniform across the site. If ground motions vary across the site it may be difficult to use PBRs as a reliable constraint on unexceeded peak ground accelerations.

Publications from this research include: one manuscript in review at the ASCE journal *Natural Hazards Review* (2011), three abstracts at Southern California Earthquake Center Meeting, Palm Springs, CA (2009, 2010) and American Geophysical Union Annual Meeting, San Francisco, CA (2010), and an invited talk presented by C. Neighbors at the Loma Linda School of Public Health (2011).

## 1. Sensitivity analysis of FEMA HAZUS Earthquake Model

### 1.1 Manuscript Publications

C.J. Neighbors, E.S. Cochran, Yuko Caras, G. R. Noriega. Sensitivity analysis of FEMA HAZUS Earthquake Model using seismic events affecting King County Washington, Natural Hazards Review, submitted, 2011.

### *1.2 Meeting Abstracts*

Neighbors, C.J., Cochran, E.S., (2010) Sensitivity analysis of the FEMA HAZUS-MH MR4 earthquake model using seismic events affecting King County Washington, AGU Abstract, American Geophysical Union Annual Meeting, San Francisco, CA

Neighbors, C.J., Noriega, G.R., Caras, Y., Cochran, E.S., (2010) Evaluating Seismic Risk using the FEMA HAZUS-MH MR4 Earthquake Model in King County Washington, SCEC Abstract, Southern California Earthquake Center Meeting, Palm Springs, CA

### 1.3 Results

*Text below is from the manuscript submitted to Natural Hazards Review on 11 May 2011 that is currently under review.*

## 1. Introduction to HAZUS

HAZUS is a widely-used risk-estimation software that provides a standardized methodology for assessing potential losses from earthquakes, floods, and hurricanes. HAZUS software operates on Geographic Information Systems (GIS) technology to calculate potential physical, economic, and social impacts of disasters. Primary users of HAZUS, such as government officials, GIS specialists, and emergency managers, use the software to develop mitigation and recovery plans as well as preparedness and response procedures for a suite of natural hazards. FEMA asserts that for State, Indian Tribal, and local governments to receive non-emergency disaster assistance, the governing body must have a standing hazard mitigation plan (*FEMA 2010*). Hazard mitigation funds provide support to municipalities and communities for hazard mitigation planning and the development of mitigation projects. By requiring mitigation and recovery plans and projects prior to a disaster, FEMA hopes to reduce overall risks to the population and built environment, while also decreasing the need for funding from post-event disaster declarations (*FEMA 2010*). In addition to estimating losses prior to a natural hazard, governments can run HAZUS scenarios after big events to estimate the degree of damage and to decide if federal recovery efforts may be needed. For example, some municipalities have an automated system for constructing HAZUS Earthquake Model scenarios using earthquake information provided by the USGS immediately after a reported event.

It is imperative for general non-science HAZUS users to understand the intrinsic limitations of running natural hazard scenarios within the framework of a computer model. There are many options available to construct a model within HAZUS, including inputs describing both the earthquake source and geologic site conditions. Using embedded databases, such as demographic aspects of the population, building counts and construction types, and utility and transportation lines, HAZUS users can carry out general loss estimations for a study region (*e.g. Whitman et al. 1997, FEMA 2000, 2003, 2008, 2010*). These loss estimates are presented in

terms of economic and social losses. As is inherent to any model, there are many uncertainties due to approximations and simplifications that are necessary for comprehensive analyses. It is best practice to test model accuracy using real world data; however, there have been few large earthquakes near U.S. urban centers in the last decade yielding few rigorous tests of the HAZUS Earthquake Model. FEMA notes that uncertainties in the HAZUS loss estimation model arise from incomplete scientific knowledge concerning earthquakes and their effects upon buildings and facilities (*FEMA 2003)*. Limitations also arise from incomplete or inaccurate inventories of the built environment, demographics and economic parameters within the embedded database. FEMA determines that these factors can result in a range of uncertainty in loss estimates produced by the HAZUS-MH Earthquake Model, possibly *at best* a factor of two or more (*FEMA 2003)*. *Price et al.* (2010) conducted a source sensitivity study in Nevada and found that uncertainty in source characteristics can result in output variations often within a factor of five, but can be up to a factor of thirteen.

This study uses the HAZUS-MH MR4 Earthquake Model. Previous studies have considered the effects of changing earthquake source and ground motion functions on HAZUS outputs and some compared their results to outcomes resulting from an earthquake occurrence (*Bendimerad 2001; Comartin-Reis 2001; Eguchi and Seligson 2008*). *Field et al.* (2005) varied both earthquake magnitude and attenuation function for a probable earthquake on the Puente Hills fault beneath Los Angeles and calculated a range of total economic loss between $82 and $252 billion. *Field et al.* (2005) note that, like the choice of earthquake source parameters such as epicenter location and moment magnitude, the choice of an attenuation relationship represents epistemic uncertainty, as the user does not know which attenuation relationship best predicts ground motion at a location. To assess ground motion accuracy in HAZUS, *Kircher et al.* (2006a) compared HAZUS-modeled scenarios for the 1994 Northridge earthquake and found that HAZUS (including soil site effects) underestimated the ground motion observed during the earthquake. *Price et al.* (2010) compared the impact of varying such inputs as epicenter location, hypocentral depth, magnitude, and fault plane dip for selected cities in Nevada. Previous studies (*Kircher et al. 2006a; Price et al. 2010*) found that the variation across model scenarios depends on the HAZUS output examined; for example, there is more variation in estimated number of casualties than building damage or total economic loss. Similar findings were found by *Kircher et al.* (2006b) and *Shoaf and Seligson* (2011). In this study, we vary inputs for the earthquake source, such as epicenter location, hypocentral depth, magnitude, and fault plane orientation and dip, as well as geologic site conditions and examine resulting variations in peak ground acceleration (PGA) and economic building damage (EBD). By conducting a sensitivity analysis of earthquake source and site conditions, this study aims to generate awareness of the limitations of loss estimation models and quantify variability of HAZUS scenarios for an individual earthquake event.

## 2. Introduction to the Study Region

King County, Washington has a population of over 2 million people and is the most populated county in the state. The county contains the city of Seattle that, as of 2009, has a population of over 600,000 people and is one of the largest urban cities and ports of the Pacific Northwest. *FEMA* (2008) ranks the Seattle-Tacoma-Bellevue, Washington region as 5$^{th}$ in the nation for annualized earthquake loss. The region has a high potential seismic hazard due to three types of earthquake events: (1) rupture along the length of the Cascadia subduction zone producing

roughly $M_w$ 9 earthquakes, (2) ruptures occurring deep in the subducting oceanic slab resulting in $M_w$ 6-7 events, and (3) rupture along numerous shallow faults in the region (Figure 1; *Atwater and Hemphill-Haley 1997, Goldfinger et al. 2003, Nelson et al. 2006, Bucknam et al. 1992, Atwater and Moore 1992*). In the past century, this area has experienced four deep (~55 km), plate boundary intraslab earthquake events: the 1949 $M_w$ 6.8 Olympia, 1965 $M_w$ 6.5 Seattle-Tacoma, 1999 $M_w$ 5.8 Satsop and the 2001 $M_w$ 6.8 Nisqually event. There have also been earthquakes on active shallow crustal faults within the Puget Sound area, the Mount St. Helens volcanic complex to the south, and other major fault systems in the region. In particular, the Seattle Fault zone is a 4-7 km wide zone of blind shallow thrust faults with slip rates estimated to be 0.7-1.1 mm/yr in the Puget Sound and Seattle urban center (*Danes et al. 1965, Johnson et al. 1999, Blakely et al. 2002, ten Brink et al. 2002*). This fault system forms the boundary between what is known as the Seattle Uplift and the 5-mile deep Seattle Basin and has the potential for producing a $M_w$ 7 earthquake (*Bucknam et al. 1992, Pratt et al. 1997*). As the Cascadia subduction zone earthquake is an extreme, infrequent event, we choose to focus on historic deep, intraslab events and shallow, crustal earthquakes. The largest shallow crustal events to affect the region in the last three decades are the 1981 $M_w$ 5.3 Elk Lake, 1995 $M_w$ 5.0 Robinson Point, and 1996 $M_w$ 5.1 Duvall. In total, we analyze seven historic earthquakes to determine the variability in HAZUS ground motion and building loss estimates. Thus, by conducting a sensitivity analysis of earthquake source and site conditions, this study will also propose general guidelines for non-earth science users to construct scientifically-based HAZUS models.

## 3. Ground Motion Simulation

### *3.1 HAZUS Methodology*

Earthquake hazards and risks are often communicated through maps showing predicted ground motions and resulting losses expected from potential earthquakes. HAZUS Potential Earth Science Hazards (PESH) can be used to estimate the ground motion and resulting ground failure (i.e., liquefaction, landslide and surface fault rupture) from a historic or potential future earthquake source. Ground motion estimates are functions of earthquake source, seismic wave path, and geologic site effects which contribute to the amplitude of ground shaking predicted for a given location. HAZUS estimates ground motions through the construction of source parameters such as fault depth, width, and length, seismic wave path through regional attenuation relationships, and site effects through NEHRP soil classes. The evaluation of ground motion is the top tier of calculations in the HAZUS model workflow for the purpose of calculating second tier estimates of structural damage and third tier estimates of economic and social losses.

HAZUS generates contour maps of ground motion as well as location-specific values of ground shaking, which are then used for building damage estimates and loss calculations. A standard response spectrum is used to simplify calculations needed to estimate damage and loss (*Kircher et al. 1997a, 1997b, 2006b, Eguchi and Seligson 2008*). PGA and spectral demand are determined between 0.3 and 1.0 sec; this range has been shown to be most relevant to estimate U.S. building damage (*Somerville et al. 1997*). The results of the building damage estimation are then used to predict: (1) casualties due to structural damage, including fatalities, (2) monetary losses due to building damage (i.e. cost of repairing or replacing damaged buildings and their contents); (3) monetary losses resulting from building damage and closure

(e.g., losses due to business interruption); (4) social impacts (e.g., loss of shelter); and, (5) other economic and social impacts (*FEMA 2003*). Economic loss from property damage is calculated as a fraction of total building exposure (*FEMA 2003*). The accuracy of estimated losses is related to the accuracy of inventory building data as HAZUS develops total building exposure from estimates of square footage and building cost data (*Kircher et al. 2006b*).

In this study, we use HAZUS-MH Maintenance Release 4 built on the platform of ESRI ArcGIS 9.3.1 with King County as the study area extent. We run all models using "out-of-the-box" population and building inventory from the U.S. Census Bureau 2000 census data (Figure 2). To simplify building damage estimates for the general building stock (e.g., residential, commercial, industrial, religious, government, educational buildings), HAZUS aggregates the general building stock and computes the damage state probability at the centroid of a census tract. Using the HAZUS built-in U.S. Census Bureau 2000 census data, King County has a total area of 5896.6 sq km and contains 373 census tracts, which range in area from 0.2 to 1478.1 sq km (Figure 2). Other studies have developed methods which allow for calculating damage at the census block level or higher-resolution grids (*Wong et al. 2005, Moffatt and Cova 2010*); however, as is noted by *Price et al.* (2010), calculations performed at smaller scales can take considerably longer to run and in the event of a large earthquake, emergency responders may not have the time or need for such a high resolution estimate.

### *3.2 Methodology*

We construct models of the 1949 $M_w$6.8 Olympia, 1965 $M_w$6.6 Sea-Tac, 1999 $M_w$5.8 Satsop, and 2001 $M_w$6.8 Nisqually deep intraslab earthquakes and the 1981 $M_w$5.3 Elk Lake, 1995 $M_w$5.0 Robinson Point, and 1996 $M_w$5.1 Duvall shallow crustal earthquakes to examine the variation in HAZUS models. We investigated three source implementations: one source supplied by the HAZUS historic catalog, and two sources that are defined by user inputs. We also run each of the three source events using two different types of geologic hazard parameters: HAZUS default inputs and user-supplied inputs for the NEHRP soil class, liquefaction susceptibility, and regional water depth parameters. For each scenario computed for an earthquake we compare two HAZUS outputs: the variation in ground motion (peak ground acceleration, PGA) and economic building damage (combined structural and non-structural damage, EBD)

#### *3.2.1 Source Model Input*

The HAZUS software constructs an earthquake source using simple parameters such as epicenter location, depth, fault plane width, orientation, and dip, and surface and subsurface rupture. Fault rupture is assumed to be of equal length on each side of the epicenter (e.g. bilateral rupture) using a finite-fault approach (*FEMA 2003, Silva et al. 2003*). We conduct a parameter test to determine the range of outputs resulting from changing these most basic source parameters. HAZUS includes a built-in earthquake catalog compiled by the USGS. The catalog contains source parameters for a historic earthquake and is useful for users who wish to model a historic event but do not have the earth science background needed to construct the event as an "arbitrary", user-defined event. For each earthquake event, we ran one "default" source from the HAZUS historic catalog and two sources that are "user-defined" by overriding the default parameters with characteristics unique to the earthquake (Tables 1 and 2).

It is important to note that when a user chooses to run a "default" source, or an earthquake from the HAZUS catalog, for some source parameters, such as the earthquake depth, a discrepancy between the catalog listing and the source input may occur. We consider this to be a database error in the HAZUS program that a general user may not notice or know to change, and thus we did not correct the error in our source input scenarios. For the other source implementations, we use a "user-defined" source by inputting source parameters for the seven earthquakes based on solutions from the global CMT (Centroid Moment Tensor) catalog *(http://www.globalcmt.org/)* and published independent studies. The first user-defined source (Source Scenario 2-1) uses the estimated fault plane and the second user-defined source (Source Scenario 2-2) uses the auxiliary plane. For these two user-defined scenarios, source parameters such as epicenter location, depth, surface and sub-surface rupture are held constant and only the fault plane orientation and dip are modified. The general HAZUS user may not know which fault plane is more correct for a specific earthquake faulting mechanism, thus by inputting both the true fault plane and the auxiliary plane we more explicitly test the importance of accurate seismologic parameters in constructing a HAZUS source event.

The seven earthquake sources include the four largest deep instraslab earthquakes and three largest shallow crustal earthquakes to affect King County in the last 30 years. The deep events occur in the down-going Juan de Fuca oceanic plate and have normal faulting mechanisms. These earthquakes range in moment magnitude from 5.8 to 6.8 and have relatively large fault plane dimensions that are described in published numerical modeling studies (Table 1; *Ichinose et al. 2004, 2006*). The shallow events occur in the North American continental crust on fault systems to the north, south, and west of the county and range in moment magnitude from 5.0 to 5.3 with differing faulting mechanisms (Table 2). The 1981 $M_w$5.3 Elk Lake earthquake occurred on a right-lateral strike-slip fault that is part of the Mount St. Helens north-south trending fault system (*Grant et al. 1984*). The 1995 $M_w$5.0 Robinson Point earthquake occurred on a reverse fault that is part of the east-west trending Seattle fault system (*Dewberry 1996*). The 1996 $M_w$5.1 Duvall earthquake occurred on a reverse fault that is part of an little-known fault system north of King County (*Pacific Northwest Seismic Network, http://www.pnsn.org/*). None of the earthquakes have known surface expressions, and thus for the mandatory surface length parameter we used the smallest possible value, 0.1 km, allowable in HAZUS.

### *3.2.2 Site Model Input*

We also vary the geologic site input to determine the overall sensitivity to both source and site parameters. HAZUS methodology uses site conditional hazards that can be input as either a singular hazard value or mapped site-specific value to estimate seismic risk. Some of these site hazards include peak ground acceleration and spectral acceleration contours, NEHRP soil classifications, and landslide- and liquefaction-susceptibilities (*Whitman et al. 1997*). NEHRP classes are based on the average shear wave velocity of the upper 30 m of the geologic material. Liquefaction is a type of soil behavior that occurs when saturated soil loses strength due to pore-water pressure changes during ground shaking. For liquefaction hazards, the probability of liquefaction occurring is a function of ground shaking amplitude (PGA), ground shaking duration as reflected by earthquake magnitude, and groundwater depth. The HAZUS methodology includes relationships between liquefaction probability based on the liquefaction-susceptibility rating and the peak horizontal PGA at a site. HAZUS uses a qualitative susceptibility rating from 0-5 (very low to very high) that is highly dependent on properties of the site geology (e.g. *Youd and Perkins 1978)*. For landslide hazards, the HAZUS methodology uses the landslide-susceptibility rating, the PGA, and the duration of ground shaking for a site to

determine if the critical acceleration of the sliding mass has been exceeded resulting in downslope displacement (*FEMA 2003).* A landslide occurs when the static plus inertia forces of a mass on a hillslope cause the factor of safety (*F*) to temporarily drop below 1.0. HAZUS uses a qualitative landslide-susceptibility rating from 1-10 (low to high) based on the relationships between geology, groundwater level and slope angle as proposed by *Wilson and Keefer (1985)*.

HAZUS users may have varying levels of geologic hazard data for a study region, thus each source model can be run with geologic hazard input variations in local NEHRP soil class, liquefaction susceptibility, and regional water depth. The site scenarios include two end-member models characterizing geologic hazards: HAZUS default values and mapped site-specific values of geologic hazards. Default values for HAZUS-MH MR 4 are defined as NEHRP soil class D (stiff soil, $180<V_s<360$ m/s), liquefaction susceptibility rating of 0 (none), and a ground water depth of 5 m. For the site-specific scenarios, NEHRP Soil Classification and Liquefaction Susceptibility maps for King County were made available by the County as mapped by the USGS. These site-specific scenarios also update the default ground water depth from 5 m to 17.3 m based on an average depth from well data provided by the County. Well data consisted of the last recorded well depth reading over the past century (1901 - 2005) for roughly 4,500 wells in and immediately adjacent to King County (*USGS National Water Information System, http://waterdata.usgs.gov/nwis*). Due to the current unavailability of HAZUS-ready landslide-susceptibility ratings for King County, we did not use this ground failure map in the analysis. In the absence of a landslide-hazard map, the landslide susceptibility rating is kept at 0 (none) for all site scenarios.

When conducting deterministic earthquake event scenarios, a user selects a predefined HAZUS attenuation relationship that is dependent on the geographic location of the study region and, for Western U.S. (WUS) studies, the faulting scenario. Attenuation describes the decrease in amplitude of ground shaking with increasing distance from the earthquake epicenter. Regional geologic characteristics influence the rate at which ground motion attenuates with distance, thus users choose an attenuation function to predict ground shaking based on knowledge of the study area and source type. HAZUS allows for individual attenuation functions to be chosen for scenarios; however ground motion estimation requires advanced knowledge of earth science, engineering and probabilistic methods. We assume that general HAZUS users, primarily emergency responders, do not have the expertise required to choose one of the more specific attenuation functions; thus, the combined attenuation relationships were chosen in this study.

For the subduction-zone events modeled, we use the 'WUS Deep Event ( > 35 km in depth)' HAZUS cocktail attenuation relationship developed by *Frankel et al. (2002).* This attenuation relationship uses the attenuation functions determined by *Youngs et al. (1997)*, and *Atkinson and Boore (2002)*, which are both weighted 50% in the model calculations. The shallow crustal reverse fault events modeled in this study use the 'WUS Shallow Crustal Event - Non-Extensional' HAZUS-MH combination attenuation relationship developed by *Frankel et al. (2002).* This attenuation relationship uses the attenuation functions determined by *Abrahamson and Silva (1997)*, *Sadigh, Chang, Egan, Makdisi, and Young* (1997), *Boore, Joyner and Fumal* (1997), and *Campbell & Bozorgnia (2003)*, which are each weighted 25% in the model calculations. The shallow crustal strike-slip events use the 'WUS Shallow Crustal Event - Extensional' HAZUS-MH combination attenuation relationship developed by *Frankel et al. (2002).* This attenuation relationship uses the attenuation functions determined by *Abrahamson*

*and Silva (1997)*, *Sadigh,Chang, Egan, Makdisi, and Young* (1997), *Boore, Joyner and Fumal* (1997), *Spudich et al.* (1999), and *Campbell & Bozorgnia (2003)*, which are each weighted 20%.

## 4 Results

### 4.1 PGA and EBD Results

In HAZUS, direct and indirect predicted damages are calculated based on estimated ground motions. For all earthquake scenarios, peak ground acceleration (PGA) was computed on the default HAZUS contour grid of 100 cells per degree of latitude and longitude where one cell has an area of 0.85 sq km for the King County study region. Figure 3 shows HAZUS-computed PGA and the spatially interpolated observed ground accelerations from the USGS/PNSN Shakemap for the 2001 $M_w$6.8 Nisqually earthquake for comparison (*Wald et al. 2005*). Considering the source input (Source Scenarios 1, 2-1, 2-2), we find that the largest ground motions (0.3-0.4*g*) are predicted for HAZUS catalog historic source (Source Scenario 1) and the smallest ground motions (< 0.05*g*) are predicted for the user-defined sources, specifically the shallowly dipping auxiliary plane (Source Scenario 2-2). Examining the site inputs (Site Scenarios A and B) reveals that including a regional NEHRP soil map (Site Scenario B) results in a spatially variable pattern of ground motion due to the amplification of seismic waves in soft sediments as prescribed in the attenuation functions (Figure 3). These results are consistent for the 6 other earthquake events modeled.

We also examined model output of the estimated monetary and spatial damage that is of great importance in hazard planning and preparedness. Due to the unavailability of robust historic accounts of damage for the earthquakes scenarios used here, we could not compare the modeled output to actual damage for each event. Thus, we conducted a spatial comparison of total economic building damage (EBD) and peak ground acceleration (PGA) across the six models for a single earthquake. HAZUS calculates the two outputs at different spatial resolutions, so we first resampled the economic building damage (EBD) and peak ground acceleration (PGA) vector data into a uniform gridded cell raster format. With the data in raster format, we determine average, maximum, and minimum PGA and EBD values across the county and use map algebra to analyze spatial variability in the model scenarios. For each of the six source and site scenarios, we calculate the percent difference in total EBD and PGA normalized by the average of the six scenarios run for each earthquake (Figure 4). We find that for most scenarios there is a clear relationship between EBD and PGA such that a scenario with higher than average PGA results in higher than average EBD with the inverse relationship (lower PGA resulting in less EBD) holding true as well. However, for some scenarios, these outputs are oppositely correlated; for example, a scenario may have lower than average PGA but higher than average EBD or vice versa. For each scenario displaying this relationship, we calculate the normalized percent difference in EBD and PGA on the gridded raster cells to examine the spatial correlation between the two outputs. We use these resulting difference maps to identify areas that experience much higher or lower than average PGA or EBD. Figure 5 shows such a map for Nisqually Source Scenario 1 and Site Scenario B with an overall lower than average PGA (-17.5%) and higher than average EBD (+31.1%). Exploring these outputs spatially we find that, for this earthquake scenario, PGA is lower than average for a large portion of the study region. However, peak ground acceleration is higher than average in the areas of

soft soil where urban centers with greater building density are located, which results in higher than average EBD. Thus by spatially examining oppositely correlated PGA and EBD scenarios, we highlight the importance of including site-specific NEHRP soil maps in HAZUS model scenarios.

To determine whether source or site scenarios produce the largest variation in EBD, we consider each source scenario (1, 2-1, 2-2) and site scenario (A, B) separately. For example, we consider a source input for a given earthquake, such as the Scenario 1 HAZUS historic catalog source, and compare the EBD predicted for the two site input scenarios (A and B). Specifically, we compare the maximum and minimum EBD (in millions of dollars) and compute the standard deviation for each set of source or site scenarios (Table 3). For the deep earthquakes, we find the largest variations while holding a site scenario fixed and varying the source inputs. For the 1949 $M_w$6.8 Olympia earthquake the largest variation, $0.65 to $1.78 million with a standard deviation of $0.57 million, occurs when we consider Source Scenario 1 from the default HAZUS catalog and vary the site scenario inputs. The 1965 $M_w$6.6 Sea-Tac earthquake has the largest variation, $1.37 to $11.31 million with a standard deviation of $5.0 million, when we consider Site Scenario B (NEHRP soil map) and vary the source scenario inputs. For the 1999 $M_w$5.8 Satsop earthquake the largest variation, $0.00015 to $0.0027 million with a standard deviation of $0.0013 million, occurs when we consider Site Scenario A (default NEHRP soil class D) and vary the source scenario inputs. The most recent deep earthquake, the 2001 $M_w$6.8 Nisqually earthquake, is similar to the 1949 $M_w$6.8 Olympia earthquake and has the largest variation, $0.61 to $2.02 million with a standard deviation of $0.70 million, when we consider Source Scenario 1 from the default HAZUS catalog and vary the site scenario input. We find similar results for the shallow earthquake events, despite more variable hypocenter depths and epicenter locations of varying azimuthal direction relative to the County. For the 1981 $M_w$5.3 Elk Lake earthquake the largest variation, $0.00054 to $0.013 million with a standard deviation of $0.0063 million, occurs when we consider Site Scenario A and vary the source scenario inputs. The 1995 $M_w$5.0 Robinson Point earthquake has the largest variation, $0.24 to $0.65 million with a standard deviation of $0.20 million, occurs when we consider Source Scenario 1 and vary the site scenario inputs. For the 1996 $M_w$5.1 Duvall earthquake the largest variation, $0.020 to $11.31 million with a standard deviation of $5.6 million, occurs when we consider Site Scenario B and vary the source scenario inputs. For each earthquake we also compute the ratio between the maximum and minimum EBD for all scenario runs. For the seven earthquakes, this factor varies between 3.3 and 566, with a median value of 6.6. The factor of 566 occurs across Duvall earthquake Source Scenarios 1 and 2-2 for Site Scenario B and is most likely due to a significant difference in the HAZUS catalog magnitude of 5.8 and user-defined magnitude of 5.1 in addition to other differences in source inputs such as epicenter location and fault area and orientation. Compiling the total range in EBD for each input scenario, we determine how the EBD varies across all earthquakes while holding either the source or the site input fixed (Figure 6). We find that modifying the source input produces the largest overall variation in economic building damage; however, there is also a significant variation in EBD predicted when using the HAZUS historic catalog event and modifying the site input.

### *4.2 Comparison of HAZUS Output to Observations for the Nisqually Earthquake*

While robust estimates of recorded ground motion and damage do not exist for all the historic earthquakes modeled in this study, we do have limited recorded data available for the Nisqually earthquake. For the 2001 $M_w$6.8 Nisqually earthquake, we briefly compare the estimated ground

motion for the six HAZUS scenarios to the USGS/PNSN Shakemap, which is based on ground accelerations observed at existing seismic stations and interpolated over the study area (*Wald et al. 2005*). We find that the ground motions estimated for the user-defined source events more closely resemble the recorded peak ground accelerations than those produced by the default HAZUS catalog source (Figure 3). And, comparison of the site input scenarios to the Shakemap show that inclusion of a regional NEHRP soil map (e.g. Site Scenario B) more accurately reflects the overall spatial variation in PGA; although, the amplitudes of the Site Scenario B PGAs are lower than observed values.

We also ran the six Nisqually scenarios using the HAZUS Advanced Engineering Building Module (AEBM) for the King County Youth Services (YSC) building in Seattle. As the YSC is a government building, construction type and other building properties are of public record and can be implemented into the AEBM model. Building value was derived from the King County Department of Assessments and HAZUS building construction type, 'Steel Frame with Unreinforced Masonry Walls', was determined by building plans provided by the Seattle Department of Planning and Development. Monetary damage estimates due to the Nisqually earthquake were provided to us by Washington State's Emergency Management Division. The Emergency Management Division reports the YSC sustained $87,314 in damages. AEBM YSC models for the default source with varying site conditions scenarios range from $166,550 to $311,590 (overestimates by a factor of 1.9 to 3.6) while user-defined source scenarios are more accurate and range from $70,240 to $85,470 for the fault plane and auxiliary plane sources, respectively. Because more detailed EBD reports for the Nisqually earthquake are not available we cannot provide a more comprehensive analysis of actual versus predicted EBD in King County.

## 5. Discussion and Conclusions

In this study we determine the variation in HAZUS-model predicted PGA and EBD for both shallow crustal and deep intraslab events affecting King County, Washington. For each of the seven earthquakes, we vary source inputs and site inputs to examine HAZUS sensitivity to changes in source parameters and site effects. We find that using a default earthquake source from the HAZUS catalog of historic events usually produces higher PGA than the user-defined sources (Figure 3). This discrepancy is most likely due to errors in the HAZUS default catalog, such as source depth and magnitude. HAZUS does not appear sensitive to the orientation of the rupture plane if the fault does not rupture to the surface. This finding is expected considering that HAZUS Methodology models an earthquake as a simple bilateral rupture on a finite fault.

For local geologic hazards, we find that using the default singular hazard value (NEHRP Soil Class D) tends to produce higher than average PGA and EBD; conversely using a site specific NEHRP soil and liquefaction susceptibility map produces lower than average PGA and EBD (Figure 3). The local NEHRP soil map has more variability in soil type including stiff soils and bedrock, geologic materials that would cause little to no amplification of seismic waves and therefore less damage to the built environment. We would expect that PGA and EBD should roughly scale, such that as the PGA increases so too should EBD. However, for some model scenarios we find that, for example, when PGA is lower than average, the EBD is higher than average. We attribute the oppositely correlated PGA and EBD to the spatial distribution of PGA values relative to the population centers (e.g. potential loss regions) for different scenarios (Figure 4). For example, in scenarios where higher than average ground motions (due to soft

sediments) coincide with a high density built environment we find higher than average property damage (Figure 5). For King County, several large cities are located on soil classes that are likely to amplify ground motion and thus experience greater losses. From these observations, it is clear that HAZUS models should include local geologic site conditions when available. However, it is important to note that inclusion of site-specific maps results in computation times at least twice that of singular site values for the study region.

We consider the range in economic building damage (EBD) for the various source and site scenarios in this study. We find that the largest variation in predicted EBD is due to modifying source parameter inputs within Site Scenario B (Tables 1 and 2, Figure 6). This is due to the spatial variability and overall amplitude of ground motion, e.g. high PGA coupled with soft sediments underlying urban centers results in very large predicted EBD for Source Scenario 1, but significantly less damage is predicted for the more moderate shaking produced by Source Scenario 2-2. This variation may also be due to modifying the location of the earthquake epicenter relative to urban centers and is explored more robustly in *Price et al.* (2010). We also see a large variation in EBD when using historic HAZUS catalog earthquake source (Source Scenario 1) with varying site parameters. Using the singular HAZUS default NEHRP soil class (Site Scenario A) for the region isometrically smears grounds motion across the study region in a radial pattern away from the epicenter of the source causing a potentially large area to be exposed to damaging ground motions. However, the inclusion of a NEHRP soil map (Site Scenario B) delineates specific areas of the built environment that may be exposed to amplified ground motions. We provide a specific comparison between scenarios using the AEBM model of the YSC and find that using the default source (Source Scenario 1) with varying site conditions (Site Scenarios A and B) overestimates by a factor of 1.9 to 3.6 while user-defined source scenarios (Source Scenarios 2-1 and 2-2) are within a factor of 1.2 to actual reported damage.

Based on the earthquake scenarios run in this study, we conclude that the user-defined sources with user-supplied geologic maps produce more accurate results. Due to significant database errors in the USGS source catalog, we encourage general HAZUS users to confer with earth scientists to construct accurate earthquake sources. As a result of the large variation in HAZUS estimated ground motions, we strongly suggest general users incorporate geologic maps in all earthquake scenarios to produce more accurate estimated ground motions relative to seismically measured ground motions.

While using HAZUS built-in inventory from U.S. Census Bureau's 2000 census data is appropriate for the events modeled in this study, for modern disaster mitigation and planning purposes the building inventory should be updated to produce more robust estimates of damage and loss. Currently it is uncertain when HAZUS will incorporate U.S. Census Bureau 2010 census data, thus future work involves updating the essential facility data (government, education, emergency response, etc. structures) and general building stock inventory for future scenario runs. Risk estimation modeling is limited by current knowledge of the system, thus ground motion attenuation functions and structural damage functions are constantly being updated. More advanced HAZUS users may wish to forego in-box HAZUS attenuation functions in favor of using user-supplied ground motion hazard maps in the form of USGS Shakemaps (when available) or constructing state-of-the-art ground motion models using OpenSHA (*http://www.opensha.org/, Field et al. 2003*). In addition to the benefit of updated ground motion prediction equations, inputting a user-supplied ground motion maps may reduce the uncertainty in the ground motions as well in the damage estimates based on building fragility functions. With

these recommendations in mind, emergency managers and other general HAZUS users should always identify their objectives to determine which inputs are most important for earthquake scenarios in their study region.

## *6. Acknowledgements*

This work greatly benefitted from discussions with Hope Seligson, Phillip McCormick, and Kevin Mickey. We are also grateful to Washington State and King County personnel for sharing the project and associated data, especially the staff at the Microfilm Library of the Seattle Department of Planning and Development, Gary Urbas at the Washington Emergency Management Division and Isabelle Y. Sarikhan at the Washington Department of Natural Resources. This work was supported partially by the U.S. Geological Survey National Earthquake Hazards Reduction Program (USGS NEHRP 2010-0019).

## *7. References*

Abrahamson, N.A., and Silva, W.J. (1997). "Empirical Response Spectal Attenuation Relationships for Shallow Crustal Earthquakes." *Seismological Research Letters*, 68(1), 94-127.

Atkinson G.M., and Boore, D.M. (2002). “Empirical Ground-motion Relationships for Subduction Zone Earthquake and their Application to Cascadia and Other Regions.” *Bulletin of the Seismological Society of America,* 93, 1703 - 1729.

Atwater, B.F., and Moore, A.L. (1992). "A Tsunami about 1000 years ago in Puget Sound, Washington." *Science*, 258, 1614-1617.

Atwater B.F., and Hemphill-Haley E. (1997). "Recurrence intervals for great earthquakes of the past 3500 years at northeastern Willapa Bay,Washington." *US Geol. Surv. Prof. Pap*, 1576, 108.

Bendimerad, F. (2001). "Loss estimation: a powerful tool for risk assessment and mitigation." *Soil Dynamics and Earthquake Engineering*, 21, 467-472.

Blakely, R.J., Wells, R.E., Weaver, C.S., and Johnson, S.Y. (2002). "Location, structure, and seismicity of the Seattle fault zone, Washington: Evidence from aeromagnetic anomalies, geologic mapping, and seismic reflection data." *Geological Society of America Bulletin*, 114,169-177.

Boore, D. M., Joyner, W.B., and Fumal, T.E. (1997). "Equations for Estimating Horizontal Response Spectra and Peak Acceleration from Western North American Earthquake: a Summary of Recent Work", *Seismological Research Letters*, 68, 128-153.

Bucknam, R.C., Hemphill-Haley, E., and Leopold, E. B., (1992). "Abrupt uplift within the past 1700 Years at Southern Puget Sound, Washington." *Science*, 258(5088), 1611-1614.

Campbell, K.W., and Bozorgnia, Y. (2003). “Updated Near-Source Ground-Motion (Attenuation) Relations for the Horizontal and Vertical Components of Peak Ground Acceleration and Acceleration Response Spectra.” *Bulletin of the Seismological Society of America,* 93(1), 314-331.

Cassidy, J.F., Rogers. G.C., Weichert, D.H. (1997). "Soil Response on the Fraser Delta to the Mw5.1 Duvall, Washington, Earthquake." *Bulletin of the Seismological Society of America*, 87(5), 1354-1361.

Comartin-Reis (2001). "HAZUS®99 SR-1 validation study." National Institute of

Building Sciences, Federal Emergency Management Agency, Washington, DC.
Danes, Z. F., Bonno, M. M., Brau, E., Gilham, W. D., Hoffman, T. F., Johansen, D., Jones, M. H., Malfait, B., Masten, J., and Teague, G. O., (1965). "Geophysical investigations of the southern Puget Sound area, Washington." *Journal of Geophysical Research*, 70, 5573–5579.
Dewberry, S.R., and Crosson, R.S. (1996). "The $M_D$ 5.0 Earthquake of 29 January 1995 in the Puget Lowland of Western Washington: An Event on the Seattle Fault?" *Bulletin of the Seismological Society of America*, 86(4), 1167-1172.
Eguchi, R. T., and Seligson, H. A. (2008). "Loss Estimation Models and Metrics." *Risk Assessment, Modeling and Decision Support,* Risk Governance and Society, A. Bostrom, S. French, and Sara Gottlieb, eds., 14, Springer, 135-170.
Ellingwood, B. R., Celik, O. C. and Kinali, K. (2007). "Fragility assessment of building structural systems in Mid-America." *Earthquake Engineering & Structural Dynamics*, 36, 1935–1952.
Federal Emergency Management Agency, (2000). "HAZUS99 Estimated Annualized Earthquake Losses for the United States." Washington, D.C., FEMA 366, 32.
Federal Emergency Management Agency, (2003a). "HAZUS99 Estimated Annualized Earthquake Losses for the United States." FEMA 366, Washington, D.C.
Federal Emergency Management Agency, (2003b). "HAZUS-MH MR4 Technical Manual, Multi-hazard Loss Estimation Methodology Earthquake Model, Washington, D.C." FEMA 366, Washington, D.C.
Federal Emergency Management Agency, (2008). "HAZUS-MH Estimated Annualized Earthquake Losses for the United States." FEMA 366, Washington, D.C.
Federal Emergency Management Agency, (2010). "Hazard Mitigation Assistance Unified Guidance, Washington, D.C." FEMA 366, Washington, D.C.
Field, E.H., T.H. Jordan, and C.A. Cornell, (2003). "OpenSHA: A Developing Community-Modeling Environment for Seismic Hazard Analysis." *Seismological Research Letters*, 74(4), 406-419.
Field, E. H., Seligson, H. A., Gupta, N., Gupta, V., Jordan, T. H., and Campbell, K. W. (2005). "Loss Estimates for a Puente Hills Blind-Thrust Earthquake in Los Angeles, California." *Earthquake Spectra*, 21(2), 329-338.
Frankel, A.D., Peterson, M.D., Mueller, C.S., Haller, K.M., Wheleler, R.L., Leyendecker, E. V., Wesson, R.L., Harmsen, S.C., Cramer, C.H., Perkins, D.M. and K.S. Rukstales, (2002). *Documentation for the 2002 Update of the National Seismic Hazard Maps*, USGS Open-File Report 02-420, 110.
Grant, W.C., Weaver, C.S., Zollweg, J.E. (1984). "The 14 February 1981 Elk Lake, Washington, Earthquake Sequence." *Bulletin of the Seismological Society of America*, 74(4), 1289-1309.
Grant, L.B. and Sieh, K. (1994) "Paleoseismic evidence of clustered earthquakes on the San Andreas fault in the Carrizo Plain, California." *Journal of Geophysical Research*, 99(B4), 6819-6841.
Goldfinger, C., Nelson, C.H., Johnson, J.E., The Shipboard Scientific Party, (2003). "Holocene Earthquake Records from the Cascadia Subduction Zone and Northern San Andreas Fault based on Precise Dating of Offshore Turbidites." *Annual Review of Earth and Planetary Sciences*, 31, 555-577.
Ichinose, G.A., Thio, H.K., and Somerville, P.G. (2004). "Rupture process and near-source shaking of the 1965 Seattle-Tacoma and 2001 Nisqually, intraslab earthquakes." *Geophysical Research Letters*, 31, L10604.
Ichinose, G.A., Thio, H.K., and Somerville, P.G. (2006). "Moment Tensor and Rupture Model for the 1949 Olympia, Washington, Earthquake and Scaling Relations for Cascadia and Global Intraslab Earthquakes." *Bulletin of the Seismological Society of America*, 96(3), 1029-1037.
Johnson, S.Y., Dadisman, S.V., Childs, J.R., and Stanley, W.D., (1999). "Active tectonics of the

Seattle fault and central Puget Sound, Washington: Implications for earthquake hazards." *Geological Society of America Bulletin*, 111, 1042–1053.
Kircher, C. A., Nassar, A. A., Kustu, O., and Holmes, W. T. (1997a). "Development of building damage functions for earthquake loss estimation." *Earthquake Spectra*, 13(4), 663-682.
Kircher, C. A., Reitherman, R. K., Whitman, R. V., and Arnold, C. (1997b). "Estimation of earthquake losses to buildings." *Earthquake Spectra*, 13(4), 703-720.
Kircher, C. A., Whitman, R. V., Holmes, and William T., (2006a) "HAZUS Earthquake Loss Estimation Methods," *Natural Hazards Review*, 7(2), 45-59.
Kircher, C. A., Seligson, H. A., Bouabid, J., and Morrow, G. C. (2006b). "When the Big One Strikes Again—Estimated Losses due to a Repeat of the 1906 San Francisco Earthquake." *Earthquake Spectra*, 22(S2), S297-S339.
Langston, C.A. and Blum, D.E. (1977). "The April 29, 1965, Puget Sound Earthquake and the Crustal and Upper Mantle Structure of Western Washington." *Bulletin of the Seismological Society of America*, 67(3), 693-711.
Moffatt, S.F. and Cova, T.J. (2010). "Parcel-scale earthquake loss estimation with HAZUS: a case-study in Salt Lake County, Utah." *Cartography and Geographic Information Science*, 37,17-29.
Nelson, A.R., Kelsey, H.M., Witter R.C. (2006). "Great earthquakes of variable magnitude at the Cascadia subduction zone." *Quaternary Research*, 65, 354–365.
Pratt, T.L., Johnson, S., Potter, C., Stephenson, W., and Finn, C., (1997). "Seismic reflection images beneath Puget Sound, western Washington State: The Puget lowland thrust sheet hypothesis." *Journal of Geophysical Research*, 102, 27469–27489.
Price, J.G., Hastings, J.T., Goar, L.D., Armeno, H., Johnson, G., Depolo, C.M., Hess, R.H., Ballard, C.M., (2010). "Sensitivity Analysis of Loss-Estimation Modeling Using Uncertainties in Earthquake Parameters," *Environmental & Engineering Geoscience*, XVI(4), 357-367.
Sadigh, K., Chang C. Y., Egan, J., Makdisi, F. and R. Youngs, (1997). “Attenuation Relationships for Shallow Crustal Earthquakes based on California Strong Motion Data.” *Seismological Research Letters*, 68(1), 180-189.
Shoaf, K., and Seligson, H. (2011). "Estimating Casualties for the Southern California ShakeOut." *Human Casualties in Earthquakes Advances in Natural and Technological Hazards Research*, 29(2), 125-137.
Silva, W., Wong, I., Siegel, T., Gregor, N., Darragh R., Lee, R. (2003). "Ground Motion and Liquefaction Simulation of the 1886 Charleston, South Carolina, Earthquake." *Bulletin of the Seismological Society of America*, 93(6), 2717-2736.
Somerville, P.G., Smith, N. F. Graves, R.W., Abrahamson, N.A., (1997). "Modification of Empirical Strong Ground Motion Attenuation Relations to Include the Amplitude and Duration Effects of Rupture Directivity." *Seismological Research Letters*, 68(1), 199-222.
Spudich, P., Joyner, W.B., Lindh, A.G., Boore, D.M., Margaris, B.M., and J.B. Flecher, (1999). "SEA99: A Revised Ground Motion Prediction Relation for use in Extensional Tectonic Regimes." *Bulletin of the Seismological Society of America,* 89, 1156-1170.
ten Brink, U. S., P. C. Molzer, M. A. Fisher, R. J. Blakely, R. S. Crosson, and K. C. Creager, (2002). "Subsurface geometry and evolution of the Seattle fault zone and the Seattle basin." *Bull. Seismol. Soc. Am.,* 92, 1737–1753.
Wald, D. J., Worden, B.C., Quitoriano V., and Pankow, K.L. (2005). "ShakeMap Manual: Users Guide, Technical Manual, and Software Guide." USGS Techniques and Methods, 12-A1, 1-128, *http://pubs.usgs.gov/tm/2005/12A01*.
Whitman, R. V., Anagnos, T., Kircher, C. A., Lagorio H. J., Lawson R.S. and Schneider P.

(1997). "Development of a National Earthquake Loss Estimation Methodology." *Earth-quake Spectra*, 13(4), 643-661.
Wilson, R. C., and Keefer D. K., (1985). "Predicting Areal Limits of Earthquake Induced Landsliding, Evaluating Earthquake Hazards in the Los Angeles Region", *U.S. Geological Survey Professional Paper*, Ziony, J. I., Editor, 317-493.
Wong, I., Bouabid, J., Graf, W., Huyck, C., Porush, A., Silva, W., Siegel, T., Bureau, G., Eguchi, R., Knight, J., (2005). "Potential Losses in a Repeat of the 1886 Charleston, South Carolina, Earthquake." *Earthquake Spectra*, 21(4), 1157-1184.
Youd, T. L., and Perkins, D. M., (1978). "Mapping of Liquefaction Induced Ground Failure Potential", *Journal of the Geotechnical Engineering Division*, American Society of Civil Engineers, 104(4), 433-446.
Youngs R. R., Chiou, S. J., Silva W. L., and Humphrey J. R., (1997). "Strong Ground Motion Attenuation Relationships for Subduction Zone Earthquakes." *Seismological Research Letters,* January/February.

**Table 1:**

**1949 Olympia Earthquake**

| | Scenario 1 | Scenario 2-1 | Scenario 2-2 |
|---|---|---|---|
| **HAZUS Source Event** | HAZUS Catalog Historic Event | User-defined Event, Plane 1 | User-defined Event, Plane 2 |
| **Fault Type** | Normal | Normal | Normal |
| **Attenuation Function** | WUS Deep Event | WUS Deep Event | WUS Deep Event |
| **Location** | 47.13, -122.95[1] | 47.17, -122.62[2] | 47.17, -122.62[2] |
| **Magnitude** | 6.9 [1] | 6.8 [3] | 6.8 [3] |
| **Depth** | 10 km[1] | 60 km[3] | 60 km[3] |
| **Width** | 10 km[1] | 33 km[3] | 33 km[3] |
| **Fault Orientation** | 0 deg[1] | 0 deg[3] | 43 deg[3] |
| **Fault Dip** | 90 deg[1] | 66 deg[3] | 31 deg[3] |
| **Subsurface Length** | 38.194 km[1] | 36 km[3] | 36 km[3] |
| **Surface Length** | 30.690 km[1] | 0.1 km[1] | 0.1 km[1] |

**1965 Sea-Tac Earthquake**

| | Scenario 1 | Scenario 2-1 | Scenario 2-2 |
|---|---|---|---|
| **HAZUS Source Event** | HAZUS Catalog Historic Event | User-defined Event, Plane 1 | User-defined Event, Plane 2 |
| **Fault Type** | Normal | Normal | Normal |
| **Attenuation Function** | WUS Deep Event | WUS Deep Event | WUS Deep Event |
| **Location** | 47.40, -122.30[1] | 47.38, -122.31[6] | 47.38, -122.31[6] |
| **Magnitude** | 6.7 [1] | 6.6 [6] | 6.6 [6] |
| **Depth** | 10 km[1] | 60 km[6] | 60 km[6] |
| **Width** | 10 km[1] | 20 km [4] | 20 km [4] |
| **Fault Orientation** | 0 deg[1] | 164 deg[6] | 64 deg [5] |
| **Fault Dip** | 90 deg[1] | 70 deg[6] | 24 deg[5] |
| **Subsurface Length** | 29.242 km [1] | 20 km [4] | 20 km [4] |
| **Surface Length** | 22.962 km [1] | 0.1 km[1] | 0.1 km[1] |

**1999 Satsop Earthquake**

| | Scenario 1 | Scenario 2-1 | Scenario 2-2 |
|---|---|---|---|
| **HAZUS Source Event** | HAZUS Catalog Historic Event | User-defined Event, Plane 1 | User-defined Event, Plane 2 |
| **Fault Type** | Normal | Normal | Normal |
| **Attenuation Function** | WUS Deep Event | WUS Deep Event | WUS Deep Event |
| **Location** | 47.07, -123.37[1] | 47.10, -123.43[6] | 47.10, -123.43[6] |
| **Magnitude** | 5.8 [1] | 5.8 [6] | 5.8 [6] |
| **Depth** | 10 km[1] | 45 km[6] | 45 km[6] |
| **Width** | 10 km[1] | 20 km [4] | 20 km [4] |
| **Fault Orientation** | 0 deg[1] | 19 deg[6] | 165 deg[6] |
| **Fault Dip** | 90 deg[1] | 34 deg[6] | 61 deg[6] |
| **Subsurface Length** | 8.790 km[1] | 20 km [4] | 20 km [4] |
| **Surface Length** | 6.223 km[1] | 0.1 km[1] | 0.1 km[1] |

**2001 Nisqually Earthquake**

| | Scenario 1 | Scenario 2-1 | Scenario 2-2 | |
|---|---|---|---|---|
| **HAZUS Source Event** | HAZUS Catalog Historic Event | User-defined Event, Plane 1 | User-defined Event, Plane 2 | USGS/PNSN Shakemap |
| **Fault Type** | Normal | Normal | Normal | (Unspecified Parameter) |
| **Attenuation Function** | WUS Deep Event | WUS Deep Event | WUS Deep Event | (Unspecified Parameter) |
| **Location** | 47.11, -122.60[1] | 47.14, -122.71[4] | 47.14, -122.71[4] | 47.15, -122.73[11] |
| **Magnitude** | 6.8 [1] | 6.8 [4] | 6.8 [4] | 6.8 [11] |
| **Depth** | 10 km[1] | 56 km[4] | 56 km[4] | 51.9 km[11] |
| **Width** | 10 km[1] | 20 km[4] | 20 km[4] | (Unspecified Parameter) |
| **Fault Orientation** | 0 deg[1] | 2 deg[6] | 176 deg [6] | (Unspecified Parameter) |
| **Fault Dip** | 90 deg[1] | 73 deg[6] | 17 deg[6] | (Unspecified Parameter) |
| **Subsurface Length** | 33.419 km[1] | 20 km[4] | 20 km[4] | (Unspecified Parameter) |
| **Surface Length** | 26.546 km[1] | 0.1 km[1] | 0.1 km[1] | (Unspecified Parameter) |

**Table 1:** Source input parameters for the deep intraslab earthquake source events considered in this study. Scenario 1 represents a historic event from the HAZUS earthquake catalog. Scenarios 2-1 and 2-2

are "arbitrary" user-defined sources using parameters from global databases and published studies.

*(References: [1]HAZUS Catalog or Default HAZUS Parameter; [2]NEIC Catalog (http://earthquake.usgs.gov/regional/neic/); [3]Ichinose et al., 2006; [4]Ichinose et al., 2004; [5]Langston and Blum, 1977; [6]CMT Catalog (http://www.globalcmt.org/CMTsearch.html); [11]PNSN Shakemap Parameter)*

**Table 2:**

**1981 Elk Lake Earthquake**

| | Scenario 1 | Scenario 2-1 | Scenario 2-2 |
|---|---|---|---|
| **HAZUS Source Event** | HAZUS Catalog Historic Event | User-defined Event, Plane 1 | User-defined Event, Plane 2 |
| **Fault Type** | Strike-Slip | Strike-Slip, Right-lateral | Strike-Slip, Right-lateral |
| **Attenuation Function** | WUS Shallow Crustal Event | WUS Shallow Crustal Event | WUS Shallow Crustal Event |
| **Location** | 46.35, -122.24[1] | 46.76, -122.14[6] | 46.76, -122.14[6] |
| **Magnitude** | 5.3 [1] | 5.3 [6] | 5.3 [6] |
| **Depth** | 10 km[1] | 6.7 km[7] | 6.7 km[7] |
| **Width** | 10 km[1] | 3 km[7] | 3 km[7] |
| **Fault Orientation** | 0 deg[1] | 167 deg[6] | 80 deg[6] |
| **Fault Dip** | 90 deg[1] | 76 deg[6] | 78 deg[6] |
| **Subsurface Length** | 4.982 km[1] | 6 km[7] | 6 km[7] |
| **Surface Length** | 2.238 km[1] | 0.1 km[1] | 0.1 km[1] |

**1995 Robinson Point Earthquake**

| | Scenario 1 | Scenario 2-1 | Scenario 2-2 |
|---|---|---|---|
| **HAZUS Source Event** | HAZUS Catalog Historic Event | User-defined Event, Plane 1 | User-defined Event, Plane 2 |
| **Fault Type** | Reverse-Slip | Reverse | Reverse |
| **Attenuation Function** | WUS Shallow Crustal Event | WUS Shallow Crustal Event | WUS Shallow Crustal Event |
| **Location** | 47.39, -122.37[1] | 47.38, -122.35[8] | 47.38, -122.35[8] |
| **Magnitude** | 5.1 [1] | 5.0 [6] | 5.0 [6] |
| **Depth** | 10 km[1] | 19.6 km[8] | 19.6 km[8] |
| **Width** | 10 km[1] | 1.2 km[8] | 1.2 km[8] |
| **Fault Orientation** | 0 deg[1] | 95 deg[8] | 136 deg[8] |
| **Fault Dip** | 90 deg[1] | 25 deg[8] | 58 deg[8] |
| **Subsurface Length** | 3.451 km[1] | 1.2 km[8] | 1.2 km[8] |
| **Surface Length** | 2.254 km[1] | 0.1 km[1] | 0.1 km[1] |

**1996 Duvall Earthquake**

| | Scenario 1 | Scenario 2-1 | Scenario 2-2 |
|---|---|---|---|
| **HAZUS Source Event** | HAZUS Catalog Historic Event | User-defined Event, Plane 1 | User-defined Event, Plane 2 |
| **Fault Type** | Reverse-Slip | Reverse | Reverse |
| **Attenuation Function** | WUS Shallow Crustal Event | WUS Shallow Crustal Event | WUS Shallow Crustal Event |
| **Location** | 47.84, -121.74[1] | 47.82, -121.79[9] | 47.82, -121.79[9] |
| **Magnitude** | 5.8 [1] | 5.1 [9] | 5.1 [9] |
| **Depth** | 10 km[1] | 8 km[9] | 8 km[9] |
| **Width** | 10 km[1] | 1.3 km[10] | 1.3 km[10] |
| **Fault Orientation** | 0 deg[1] | 175 deg[9] | 183 deg[9] |
| **Fault Dip** | 90 deg[1] | 52 deg[9] | 38 deg[9] |
| **Subsurface Length** | 8.790 km[1] | 1.3 km[10] | 1.3 km[10] |
| **Surface Length** | 6.223 km[1] | 0.1 km[1] | 0.1 km[1] |

**Table 2:** Source input parameters for the shallow crustal earthquake source events considered in this study. *(References: [1]HAZUS Catalog or Default HAZUS Parameter; [6]CMT Catalog (http://www.globalcmt.org/CMTsearch.html); [7]Grant et al., 1984; [8]Dewberry and Crosson, 1996; [9]UC-Berkeley Moment Tensor Solution (http://seismo.berkeley.edu/~dreger/mtindex.html); [10]Cassidy et al., 1997)*

**Table 3:**

| Earthquakes | Source Scenarios | | | Site Scenarios | |
|---|---|---|---|---|---|
| | **1** Default | **2-1** Fault Plane | **2-2** Auxiliary Plane | **A** Default | **B** Regional Maps |
| **1949 $M_w$6.8 Olympia** Factor: 3.8 | 0.65-1.78 (0.57) | 0.47-1.31 (0.42) | 0.47-1.31 (0.42) | 1.31-1.78 (0.24) | 0.47-0.65 (0.088) |
| **1965 $M_w$6.6 Sea-Tac** Factor: 8.3 | 1.78-11.31 (4.8) | 0.46-1.37 (0.46) | 0.46-1.37 (0.45) | 0.46-1.78 (0.66) | 1.37-11.31 (5.0) |
| **1999 $M_w$5.8 Satsop** Factor: (--)* | 0.0027-0.00066 (0.0010) | 0.00-0.00063 (0.00031) | 0.000016-0.00015 (0.000069) | 0.00015-0.0027 (0.0013) | 0.00-0.00066 (0.0017) |
| **2001 $M_w$6.8 Nisqually** Factor: 3.3 | 1.97-2.02 (0.025) | 0.61-1.73 (0.56) | 0.65-1.73 (0.54) | 1.73-1.97 (0.12) | 0.61-2.02 (0.70) |
| **1981 $M_w$5.3 Elk Lake** Factor: 130 | 0.00010-0.00054 (0.00022) | 0.0039-0.013 (0.0046) | 0.0035-0.012 (0.0042) | 0.00054-0.013 (0.0063) | 0.00010-0.0039 (0.0019) |
| **1995 $M_w$5.0 Robinson Point** Factor: 5 | 0.24-0.65 (0.20) | 0.14-0.38 (0.12) | 0.13-0.37 (0.12) | 0.37-0.65 (0.14) | 0.13-0.24 (0.056) |
| **1996 $M_w$5.1 Duvall** Factor: 566 | 0.32-11.31 (5.5) | 0.020-0.064 (0.022) | 0.020-0.065 (0.023) | 0.064-0.32 (0.13) | 0.020-11.31 (5.6) |
| Black: Variation in Building Damage (Millions of Dollars)<br>Grey: Standard Deviation (Millions of Dollars)<br>** Factor not computed if the EBD is 0 for any scenario* | | | | | |

**Table 3:** Variation in Economic Building Damage (EBD) in millions of dollars across the six HAZUS scenarios examined for seven earthquake events. We calculate the variation in EBD for a given earthquake by considering one source input while varying the site conditions or considering one site scenario while varying the source conditions. We find the range of variation (black) and standard deviation (grey) for each scenario of a given earthquake. We determine the factor by computing the ratio between the maximum and minimum for all scenario runs of a given earthquake.

**Figure 1:**

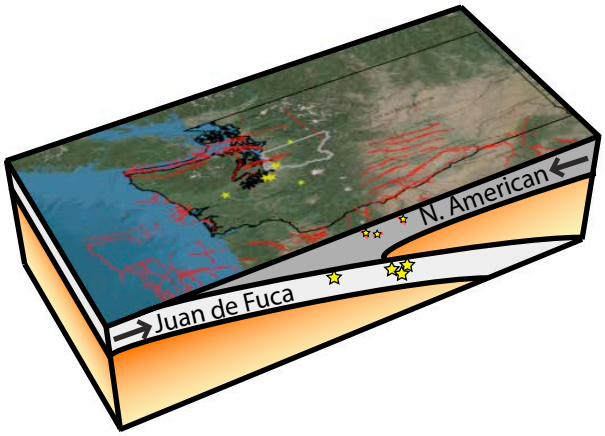


**Figure 1:** Tectonic setting of King County (outlined in grey) in relation to the Cascadia subduction zone and local faults (red lines). Locations of earthquakes that are modeled are shown as yellow stars in map view and on the cross-section schematic. Deep earthquakes occur in the down-going Juan de Fuca oceanic plate and shallow earthquakes occur in the North American continental crust.

**Figure 2:**

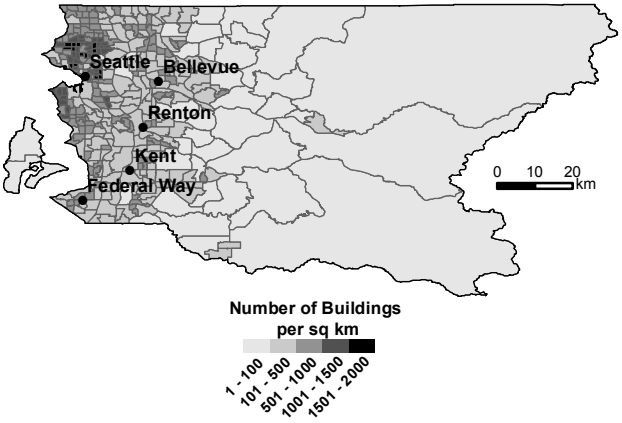


**Figure 2:** Census tract boundaries and building density (number of buildings per square kilometer) for King County based on built-in HAZUS inventory from U.S. Census Bureau 2000 census data. Locations of five most populated cities are shown (black dots).

**Figure 3:**

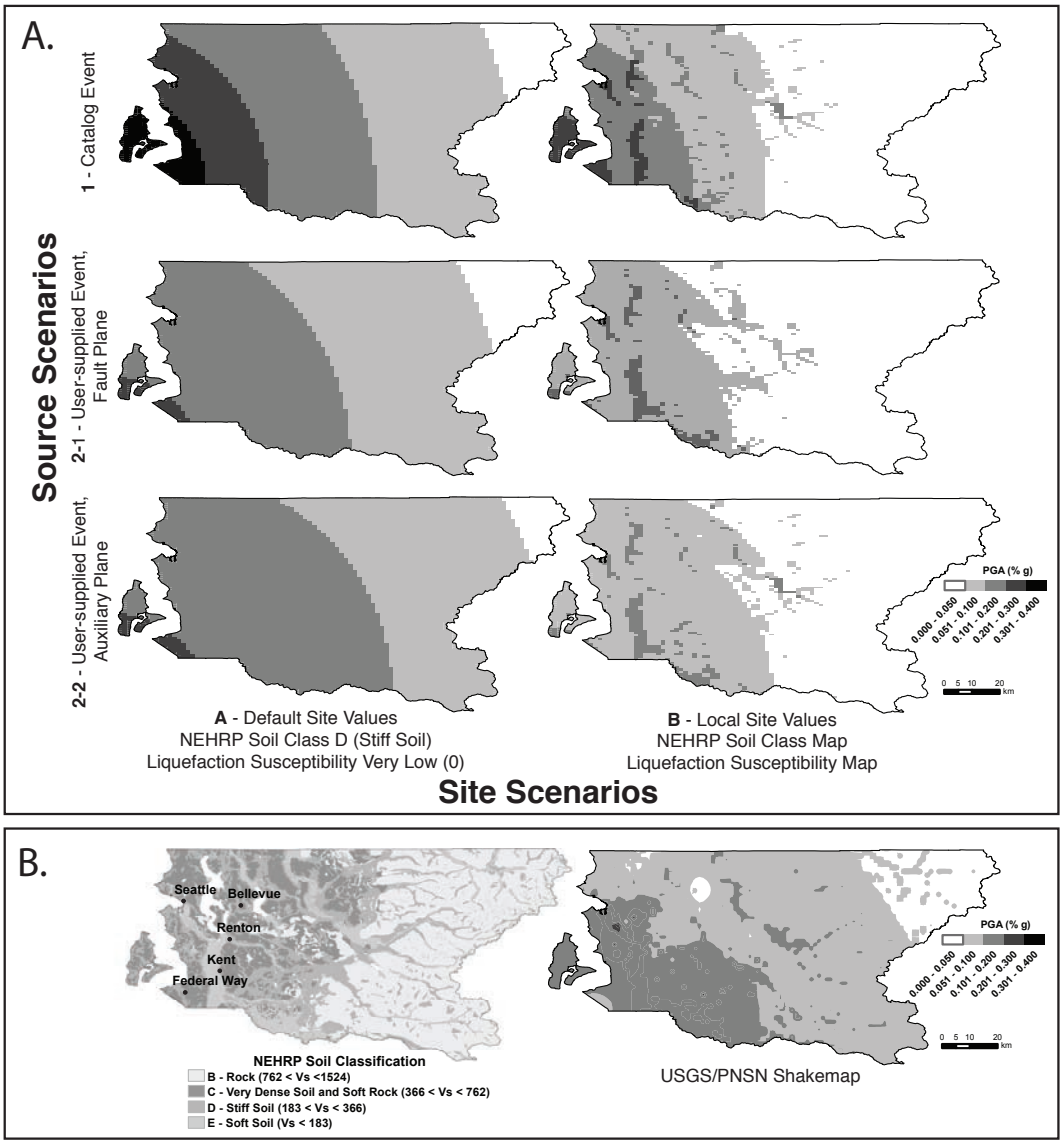


**Figure 3:** A. (Top) Maps of peak ground acceleration (PGA) for the six HAZUS scenarios computed for the 2001 $M_w$6.8 Nisqually earthquake. Top row represents historic source from HAZUS earthquake catalog. Middle and bottom rows represent arbitrary user-defined sources with preferred fault plane orientation and auxiliary fault plane orientation, respectively. Left column represents HAZUS default site values and right column represents user-supplied USGS-mapped site conditions. B. (Left) NEHRP Soil map for King County (*USGS*) (Right) USGS/PNSN Shakemap for Nisqually event showing interpolated PGA in King County.

**Figure 4:**

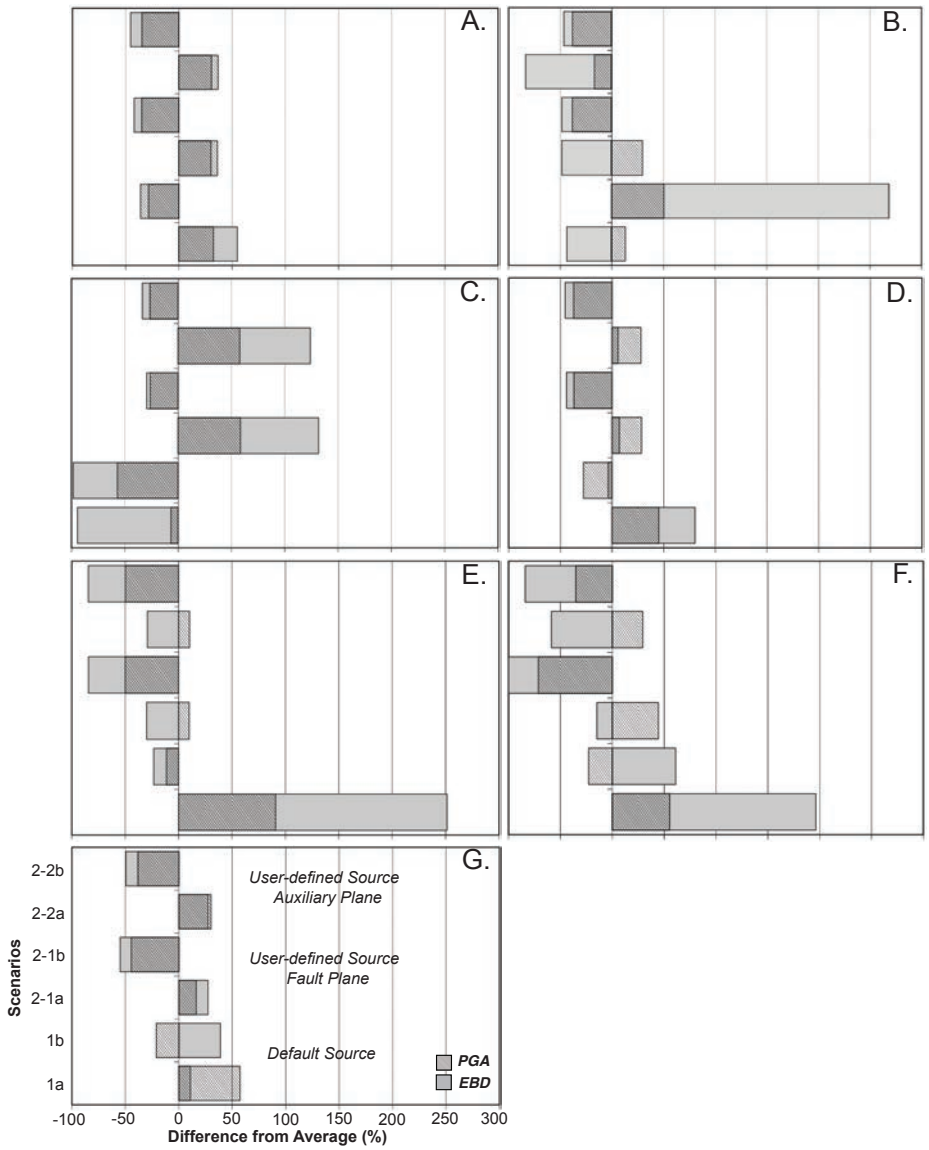


**Figure 4:** Comparison of peak ground acceleration (PGA) and economic building damage (EBD) for the 7 historic earthquakes where (A) 1949 $M_w$ 6.8 Olympia, (B) 1965 $M_w$ 6.5 Seattle-Tacoma, (C) 1981 $M_w$ 5.3 Elk Lake, (D) 1995 $M_w$ 5.0 Robinson Point, (E) 1996 $M_w$ 5.1 Duvall, (F) 1999 $M_w$ 5.8 Satsop, and (G) 2001 $M_w$ 6.8 Nisqually event. Plotted is the normalized difference in PGA or EBD from the average across the six source and site scenarios.

**Figure 5:**

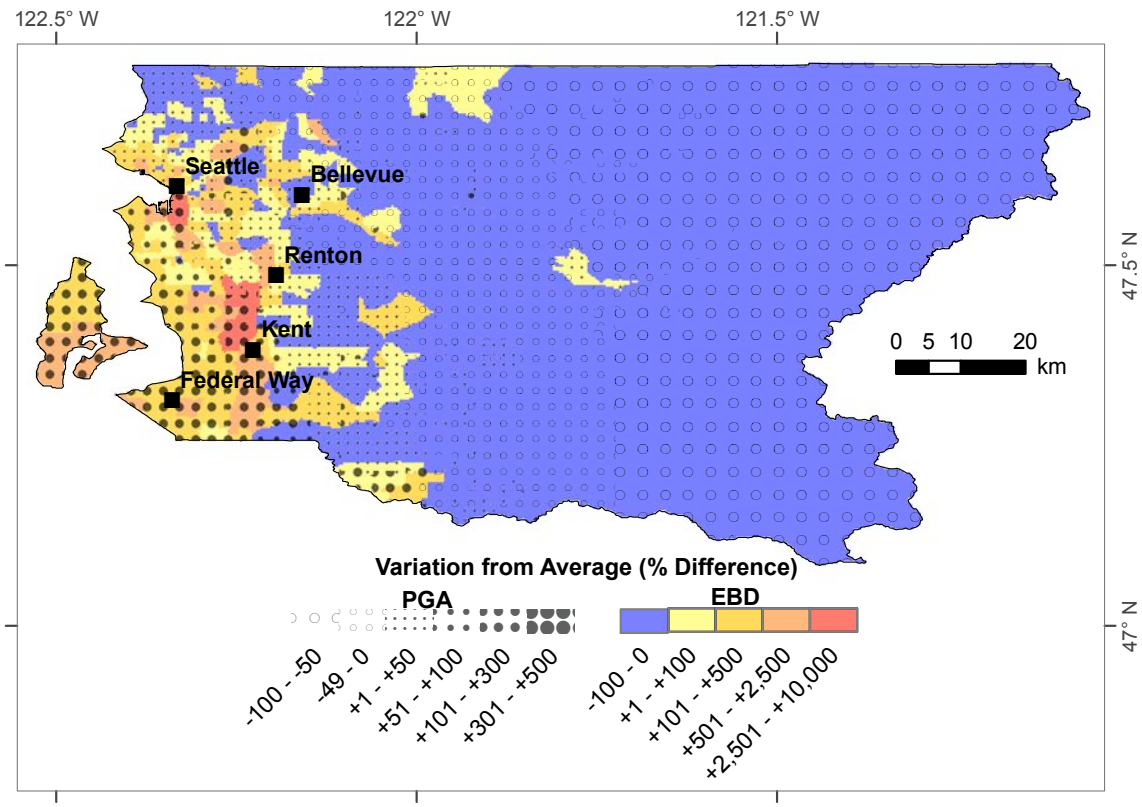


**Figure 5:** Variation in PGA (open circles represent areas of lower than average ground motion, closed circles higher than average with size of circle increasing from 0% difference) and EBD (blue represents areas of lower than average and increasingly warmer colors represent areas of higher than average EBD) for the 2001 Nisqually earthquake. Shown is the PGA and EBD estimated using Source Scenario 1 and Site Scenario B conditions (see Table 2).

**Figure 6:**

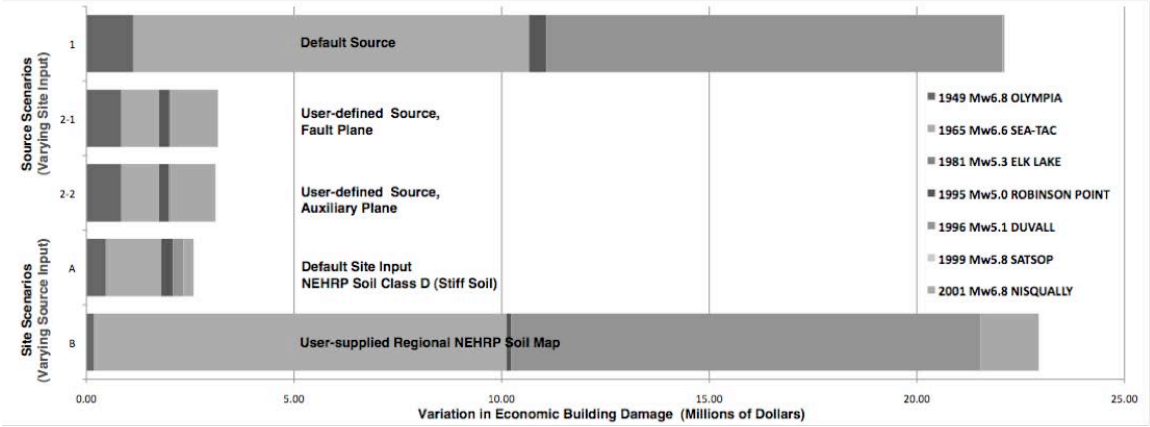


**Figure 6:** Combined variation in Economic Building Damage (EBD) for all earthquakes. The top three bars represent variations caused by changing site inputs while holding the source condition constant. The bottom two bars represent variation caused by changing source conditions while holding the site input constant.

## 2. Seismic Coherency at Precariously Balanced Rock Sites, Riverside, CA

### *2.1 Meeting Abstracts*

Neighbors, C.J., and Cochran, E.S. (2009) Assessing FEMA HAZUS-MH MR3: Constraining seismic hazard estimates for Riverside County using precariously balanced rocks, SCEC Abstract, Southern California Earthquake Center Meeting, Palm Springs, CA

### 2.2 Results

*Work completed to date and analysis will be written up for publication in a peer-reviewed journal.*

### 1. Introduction

This work will provide better estimates of maximum shaking levels for a region within 8 km of the San Jacinto fault (SJF) and other large fault systems in Southern California. For Riverside County, these faults are known to be capable of producing peak ground accelerations in excess of 0.2 g, while nearby Elsinore and Cucamonga (extension of Sierra Madre fault system) fault zones are capable of generating 0.1-0.2 g ground accelerations. Recurrence intervals for these fault systems range from roughly 150 (+123/-71) years for the San Andreas, 100 (+150/-50) years for the San Jacinto, 310 (+340/-146) years for Elsinore, and 200-700 years for Cucamonga (*Dieterich et al., 1995*). Based on these estimates of peak ground accelerations and return intervals, it is expected that precarious rocks, which are estimated to be thousands of years old, would have toppled from their current positions. It is hypothesized that these rocks still exist due to lack of strong ground motions in the time since the PBRs were exposed or due to anomalous site conditions such as deamplification of ground motion that prevent the rocks from toppling (*Stirling et al.*, 2002). The work of *Brune* (1996) documented PBRs to within roughly 15 km of the SJF (*Brune*, 1996), so the data provided here provide further constraints on the maximum acceleration estimates for the regions close to SJF. The existence of precariously balanced rocks in close proximity to the San Andreas and the San Jacinto faults, which have repeated large earthquakes, may help constrain strong ground motion estimates that may be overestimated in USGS-CDMG seismic hazard maps and within the Probabilistic Seismic Hazard Analysis (PSHA) methodology.

The study of PBRs is somewhat hampered by the question of how variable ground motion is at small spatial scales. It is possible that isolated PBRs may not accurately represent maximum accelerations across a region. It is therefore necessary to determine how variable ground motion is near PBR sites. If ground motion varies significantly on a small scale (< 1 km), then seismic hazard estimates determined using PBRs may not be a reliable method to determine maximum ground accelerations. However, if ground motion does not vary significantly, PBRs provide an additional tool to estimate the maximum accelerations expected for a region. The PBR and seismic data we propose to collect have direct application to earthquake hazard and loss assessments for the urban region of Riverside County

### 2. PBR Acceleration Estimates

We use the methods developed by *Anooshehpoor et al.* (2004) to determine the quasi-static toppling force. The quasi-static toppling force is measured by applying a horizontal force in the

direction that the boulder is most likely to topple through the estimated center of mass (Figure 1). The force is given by:

$$F_i = mg \tan\alpha_i,$$

where $m$ is the mass of the rock, $g$ is the gravitational acceleration, and $\alpha_i$ is the angle between lines though vertical and the rocking point from the center of mass.

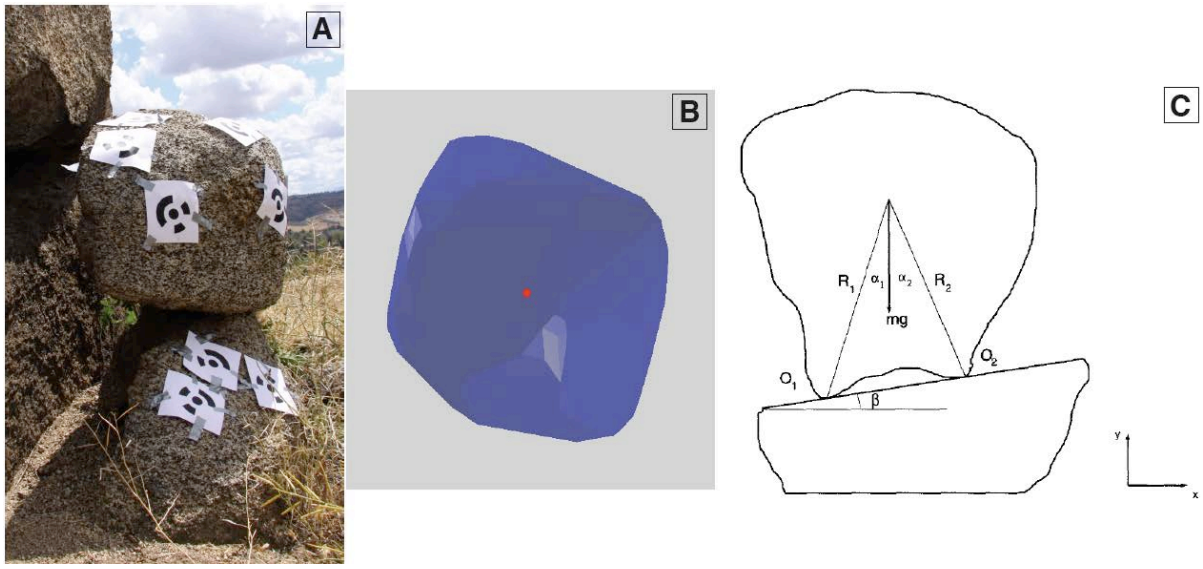


**Figure 1:** (a) One of the PBRs found on campus property with targets to create 3-D geometric shape using the Eos Systems, Inc. Photomodeler software (*photo by C. Neighbors*). (b) 3-D geometric shape with center of mass (red dot) as calculated in Matlab (model code from *M. Purvance, written communication*) (c) Two-dimensional physical model used to calculate quasi-static toppling force (figure from *Shi et al.*, *1996*).

To determine the toppling force in the field, one common method is to loop a chain around the rock at the boulder's center of mass and pull the rock slowly using a pulley connected to a truck. The chain, and thus the tensional force on the boulder, is kept horizontal by a height-adjusted, supporting metal post. The free-end of the chain has a digital load cell, which measures the force acting on the rock. As the tensional force is increased, the rock reaches a threshold where it begins to rotate about its rocking point, at which time the pulling force is slightly increased and a decrease in the magnitude of the force should be observed. A pushing technique, utilizing a hydraulic piston and load cell, can also be used to find the toppling force. The mass of the rock, $m$, is determined by estimating the density and the volume of the rock. Density is determined from lab analysis of rock samples, while volume is estimated by determining the volume of multiple cross-sections and then summing these subvolumes. Digital photogrammetry, or multiple pictures of the boulder from many reference angles, can also be utilized to determine the volume, center of mass, and the angle $\alpha$ by analysis of 3-D visual software packages such as Photomodeler by Eos Systems, Inc (Figure 1).

Contemporary investigations of overturning responses of shaken freestanding blocks, such as PBRs, utilize a probabilistic approach to determine the overturning potential of blocks exposed to earthquake ground motions (*Purvance et al., 2008a*). Previous work (*Yim et al., 1980*) has shown that overturning probability increases as the amplitude of the peak horizontal ground

acceleration increases, with increasing block slenderness, and with decreasing block size (*Purvance et al., 2005*). It has also been shown that vertical ground shaking does not significantly affect the average overturning probability (*Yim et al., 1980*). Relationships for the overturning fragilities use PGA as a function of the overturning probability, block slenderness, block height, and either the PGA normalized peak ground velocity (PGV/PGA), or the 5%-damped spectral acceleration at 1 sec ($S_{A1}$/PGA) and 2 sec ($S_{A2}$/PGA). Previous studies have also shown that variations in geometry and rock type affect the overturning fragilities. *Purvance et al.* (2008) found that granitic boulders, similar to those found near the UCR campus, have lower than predicted PGA values as there may exist complex basal contact conditions, such as multiple rocking points, rather than possessing sharp basal contacts as used in laboratory experiments.

Numerical results of *Anooshehpoor et al.* (2004) find that less precarious rocks can be more difficult to topple if they have complex rock-pedestal geometries. Less precarious boulders are also found to be more difficult to overturn as their height to width ratio decreases requiring a higher acceleration to initiate rocking motion leading to eventual overturn. In addition, smaller boulders are more sensitive to the high frequency ground motions while larger boulders are more sensitive to low frequencies. It is also important to note that the toppling force required for overturning a rock is the force in the direction that the rock is most easily overturned. This toppling direction may not be the direction of maximum ground shaking, thus in areas where there are multiple precariously balanced rocks with various toppling directions better constraints on peak ground motion can be determined (*Anooshehpoor et al.*, 2004).

We identified three precariously balanced rocks on University of California, Riverside campus to estimate toppling accelerations. Most of the identified PBRs are small boulders, ranging from 0.5 – 1.5 m in height, 0.5 - 1 m in width, and 0.5 – 1 m in length. Pictures were taken of the rocks and have been input into visualization software to estimate rock and pedestal geometry, including the center of mass, rocking points, and the fragility angle between vertical and the rocking points for the balanced rocks (*Figure 2*). We have completed initial analysis of PBR quasi-static toppling accelerations for one of the rocks using Photomodeler software to create 3-D models of the rock and pedestal configurations (*Figure 2*). For this rock we find a toppling acceleration of 3-3.96 m/s$^2$ (~31-40% *g*). For the other two PBRs we estimated the toppling acceleration from dimensions alone and find toppling accelerations between 7.67 – 10.93 m/s$^2$.

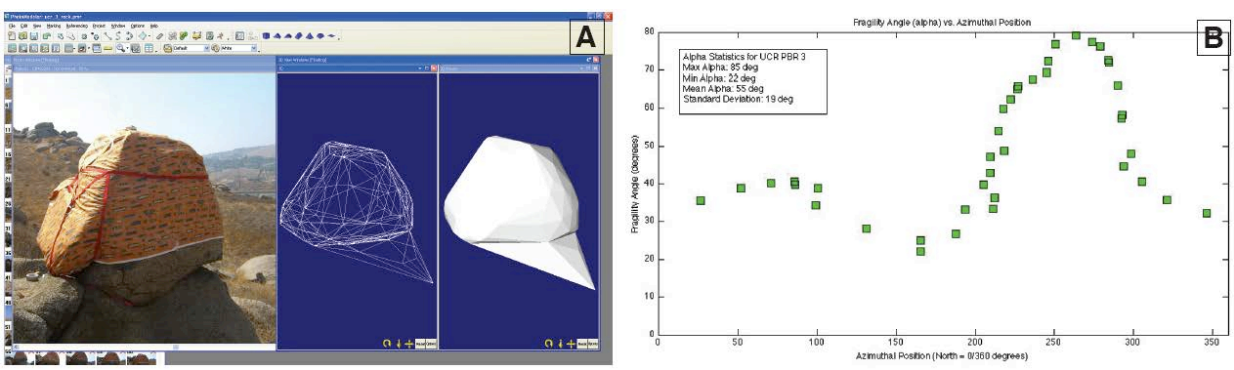


**Figure 2:** (a) 3-D geometric model of UCR PBR3 rock and pedestal (modified from *R. Anooshehpoor, written communication*) (c) preliminary fragility angle ($\alpha$) estimates relative to azimuthal direction.

### *3. PBR Dating Methods*

Cosmogenic nuclide dating will be used to constrain the age of the rock's surface exposure. Cosmogenic dating is based on the principle that high-energy cosmic rays entering Earth's atmosphere collide with nuclei, which triggers the generation of high-energy neutrons. When this collision occurs in minerals, a process known as spallation occurs as the nuclei are broken into fragments and create new nuclides. The number of nuclides within surficial rocks gives a surface exposure age for the rock, or the amount of time the rock has been exposed to cosmic-ray activity (*Walker, 2005*). To date the surface, samples are collected by chiseling off a 1-2 cm thick layer from a near horizontal surface of the rock. The cosmogenic nuclide beryllium-10 ($^{10}$Be), which has a half life of $1.5 \times 10^6$ years, is measured using Accelerator Mass Spectrometry (AMS) and is good for dating quartz grains, which is a predominant mineral in the granitic boulders we find in the region surrounding UCR (*Brown et al., 1996*). Assumptions underlying cosmogenic nuclide dating include that the surface has not had previous surficial exposure yielding some amount of inherited cosmogenic isotopes and that the surface has not been eroded or weathered since the initial exposure (*Walker, 2005*). Due to the weathered nature of balanced rocks, we interpret the calculated age as the minimum time of surface exposure.

Calculations of cosmogenic nuclide production rates at sample sites requires scaling relationships that account for variation in nuclide production rate with time, location and elevation, and a reference production rate at a particular time and space, commonly the present time at sea level and high elevation (*Balco et al.*, 2008). Using local, time-integrated production rates of nuclides at calibration sites allows for development of scaling relationships to measure local production rates. When collecting samples to determine nuclide concentrations, we will account for location (latitude and longitude), elevation, thickness, and density of each sample as well as the geometry of the surrounding area as this may be an important factor in calculating the shielding correction and erosion rate. The shielding factor corrects for topographic or other obstructions (such as surrounding rocks) that may reduce the cosmic-ray flux to the sample site. While there is no standard method for determining this factor, *Nishiizumi et al.* (1989) devised that the angular distribution of the cosmic radiation responsible for $^{10}$Be production decreases in proportion to $cos(2.3\theta)$, where $\theta$ is the zenith angle.

Sample elevation is also an important factor to record for calculations of radiogenic nuclide concentrations. Site elevation is used to determine the atmospheric depth, which is an important environment factor effecting nuclide production (*Balco et al., 2008*). Atmospheric depth controls nuclide production rates, but is a difficult factor to determine as sample sites are rarely located next to weather stations and most sample sites are older than instrumental records of atmospheric pressure therefore most modern observations do not reflect the conditions of the entire exposure period. To mitigate the errors, a standard pressure-elevation relationship can be used in combination with atmospheric approximations, such as mean sea level and temperature fields, to capture regional variations in this relationship when determining the atmospheric pressure at the site (*Balco et al.*, *2008*).

In an attempt to standardize $^{10}$Be exposure age calculations, *Balco et al.* (2008) developed the following equation to determine the measured nuclide concentration:

$$N = S_{thick} S_G P_{ref,sp,Xx} \int_0^T S_{Xx}(t) \exp(-\lambda t) \exp\left(\frac{-\varepsilon t}{\Lambda_{sp}}\right) dt + P_\mu \int_0^T \exp(-\lambda t) \exp\left(\frac{-\varepsilon t - \frac{z}{2}}{\Lambda_\mu}\right) dt$$

where $N$ is the measured nuclide concentration (atoms $g^{-1}$), $T$ is the exposure age, $S_{thick}$ is the sample thickness correction, $S_G$ is the geometric shielding correction, $P_{ref,sp,Xx}$ is the reference production rate due to spallation for scaling scheme $Xx$ (atoms $g^{-1}$ $yr^{-1}$), $S_{Xx}(t)$ is the scaling factor for scaling scheme $Xx$, $\lambda$ is the decay constant (4.62 x $10^{-7}$ $yr^{-1}$ for $^{10}Be$), $\varepsilon$ is an independently determined surface erosion rate (g $cm^{-2}$ $yr^{-1}$), $\Lambda_{sp}$ is the effective attenuation length for spallogenic production (g $cm^{-2}$), $P_\mu$ is the surface production rate in the sample due to muons (particles similar to electrons created when cosmic rays collide with particles in the Earth's atmosphere) (atoms $g^{-1}yr^{-1}$), $z$ is the sample thickness (g $cm^{-2}$) and $\Lambda_\mu$ is an effective attenuation length for production by muons (g $cm^{-2}$). The rock is sampled at regular intervals from the top of the rock to the base of the pedestal and fit with a numerical model to constrain nuclide concentration over the exhumation history of the rock (*Balco et al., 2011*). A 3-D geometric model of the rock, pedestal, and surrounding topographic features is used to calculate the shielding factor, $S_G$ (Figure 3) (*Balco et al., 2011*).

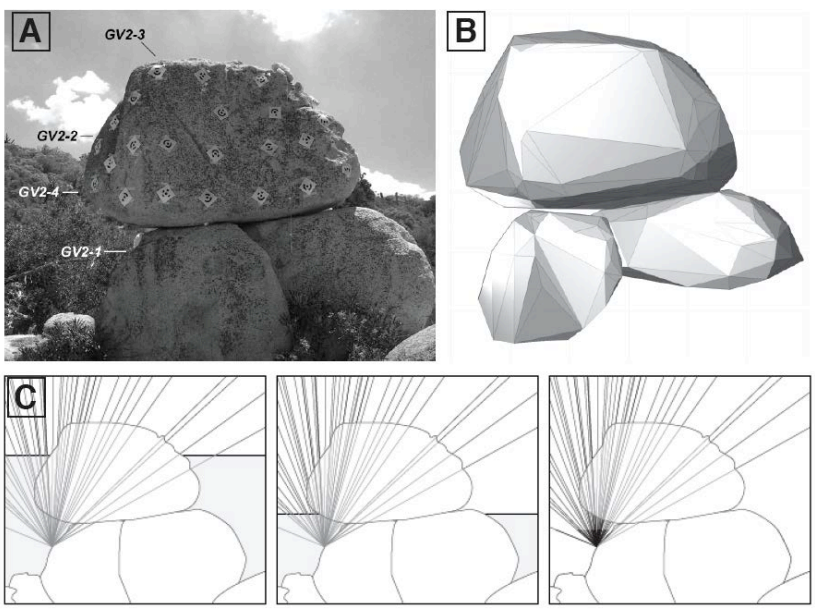


**Figure 3:** Figures from *Balco et al.* (2011) showing sampling and modeling methods. (a) Precariously balanced rock in Southern California with sample locations marked and target points for creation of 3-D geometric model (b) 3-D geometric model of rock and pedestal created in Eos Systems, Inc. Photomodeler software (c) Shielding factor simulation of rock and sediment cover during exhumation process at sample point on pedestal. Lines represent cosmic ray paths to sample point.

Errors and uncertainties lie in the difficulty of determining the accuracy of the calculation terms due to paucity of available data, uncertainties in nuclide concentrations from the AMS measurement, uncertainties in the developed scaling schemes from reference production rates, local atmospheric pressure, and magnetic field reconstructions (*Balco et al.*, *2008*). Soil samples for cosmogenic nuclide surface exposure dating are also collected from the hillside near the PBRs to establish erosion rates. The method assumes that the rock has been steadily exhumed at a fixed rate and the model fits the nuclide concentrations to the various sample locations. However, it is possible that rather than being exposed over a constant rate, the rock may experience rapid phases of exhumation (*Balco et al., 2011*). The method also models the nuclide concentrations under the assumption that the rock is *in situ* and therefore has not rolled or fallen into the current position. Lastly, the model assumes that the measured nuclide

concentrations are due to first order interaction processes between cosmic rays and the rocks and neglects any secondary nuclide particle production that may occur due to other processes (*Balco et al., 2011*).

We, in collaboration with Dylan Rood, sampled two rocks (UCR PBR 1, UCR PBR 3) for age dating in August 2010 and February 2011 (*Figure 4*). Dr. Rood is currently performing chemical analysis . His recent move to a new institution delayed the processing of the samples, but the results should be available by mid-2012.

**Figure 4:** (a) D. Rood chiseling samples from UCR PBR3 for cosmogenic nuclide dating (b) sample locations on rock and pedestal (c) drilling into UCR PBR1 to collect samples (d) sample locations on rock and pedestal (*photos by C. Neighbors*).

## 4. Seismic Coherence

The question of ground motion coherence is paramount to correctly interpret the constraints provided by this set of PBRs. Seismic wave coherency is a measurement of the variability of seismograms and ray path scattering and attenuation processes in the space-frequency domain (*Zembaty and Krenk, 1993*). Previous studies have assessed coherency, or the spatial correlation of ground motion, over sediment sites, but there are few studies of coherence over rock sites using a dense seismic array (*Tucker et al., 1984*; *Menke et al., 1990*; *Vernon et al., 1991*; *Hough and Field, 1996*). The coherence of rock sites have not been well established as most studies simply assume rock sites have little to no site amplification relative to sediment sites (*Borcherdt, 1970; Steidl et al., 1996; Boore and Joyner, 1997*). *Schneider et al.* (1992) compared the coherency functions from “rock” sites in the Peninsular Ranges with those for soil sites, finding that the “rock” sites demonstrated significantly lower coherency than soil sites in other arrays. Subsequent research showed that these “rock” sites are underlain by a highly variable topography of granite that is filled with grus (weathered granite) (*Vernon et al., 1991; Schneider et al., 1992*). In addition, “ringing” codas were observed consistent with corestones buried beneath the surface vibrating relative to the softer grus. Thus, if PBR sites are incoherent with respect to surrounding areas, then the PBRs may not provide robust constraints on the level of shaking experienced by the region due to past earthquakes. However, if PBR sites exhibit complete coherency (e.g., the ground shakes identically at all sites) then it would imply that limits can be placed on maximum ground motions for the duration of the exposure age of the rock. For this case, the set of PBRs provide a constraint only as strong as the constraint placed on the ground motions by the most easily overturned PBR.

There is presently debate in the literature as to whether PBR sites are 'typical' rock sites as recent work found that ground response at PBR sites may be highly frequency-dependent,

throwing into question the validity of using a PBR fragility estimate to constrain unexceeded ground motion (*Stirling et al., 2002; O'Connell et al., 2007*). A rigorous study of coherency in proximity to a group of PBRs is needed to assess the uncertainty associated with PBR fragility estimates. Once the coherence at the PBR sites has been assessed, it will be possible for us to rigorously test its effects on the overturning responses of PBRs. We will synthesize waveforms that conform to the observed coherence as a function of frequency and distance. By simulating the rocking and overturning responses of PBRs when exposed to the correlated sets of waveforms, we can determine the conditional probability that multiple PBRs would overturn given the waveform coherency. The seismic data collected in this study will allow us to better assess the reliability of PBR acceleration estimates by determining the small-scale variation in seismic wave amplitudes on a hard rock sites.

We compare ground motions from regional earthquakes over a 15-month period at 10 locales within 100 meters of a PBR site using PASSCAL instruments (Figure 5). Using seismic methods outlined in *Hough and Field* (1996), we determine the seismic wave coherency using the direct S-wave arrivals and correlate ground motion to subsurface site properties, including seismic velocities. Due to the close spacing of the seismic stations, we eliminate the incoherence due to multidirectional S-wave radiation patterns. The PBR and surrounding seismometer sites are located on Cretaceous age granites with a thin layer of weathered granite sediment. However, in a general sense, the study area is composed of the same geologic site material and we can conclude that the coherence will be a measurement of ground motion variability across sites of the same rock classification. For each seismic station, coherency estimates for all the station-PBR pairings will be binned and averaged to determine the significance of distance on coherency results. Thus, we will determine small-scale variability of an rock site, specifically a rock site that forms precariously balanced rocks.

To calculate coherency, seismograms for earthquakes recorded during the deployment period will be analyzed following the methods outlined in *Hough and Field* (1996). Seismograms will be corrected for instrument response to compare frequency spectra and amplitudes at various bands to estimate site amplification effects. We will use a 5-6 sec window centered around the direct S-wave arrival on the radial and transverse horizontal components for each event. Using the direct arrival will eliminate complex phases of S-wave coda and the window length is chosen due to the choice of analyzing the lower frequencies and to eliminate the need to determine the exact time duration of the direct S-wave. Due to the importance of measuring the small-scale variations in a finite-length signal, the S-wave windows that are cut from the time series data will be tapered at the ends using a multitaper method developed by *Thomson* (1982). This multitaper method has been shown to decrease spectral leakage where some power 'leaks' between frequencies and basically acts as a weighted sum of a set of single tapers to decrease the variance of the estimated signal that can occur when using a single taper method (*Prieto et al., 2007; Hough and Field, 1996; Menke et al., 1990*). Coherence is calculated at the nine radially-aligned stations relative to the PBR station following the equation stated in *Menke et al.* (1990):

$$C(f,r) = \frac{\left|\left\langle s^*(x_1,f)s(x_2,f)\right\rangle\right|^2}{\left[\left\langle s^*(x_1,f)s(x_1,f)\right\rangle\right]\left[\left\langle s^*(x_2,f)s(x_2,f)\right\rangle\right]}$$

where $s(x_i,f)$ is the Fourier transform of the $i$th time series and * denotes the complex conjugate. The angular brackets indicate the group average of the cross- and auto- power spectra. Seismologists use auto and cross power spectra to compare the power, or the average value of signal as a function of frequency, present in a signal and to a second signal, respectively. Coherency is measured on a scale of 0 to 1, where 0 represents no similarity in the responses of the two stations and 1 represents total similarity assuming that the phase differences due to wave passage and amplitude differences due to site effects are corrected between two stations and any ambient noise, such as that from power lines near a station, are removed. In general, studies find that at low frequencies over short station distances ground motion coherency approaches 1, while at high frequencies over large distances coherency tends to 0 (*Menke et al., 1990; Abrahamson et al., 1991; Zerva and Zervas, 2002*).

For the coherency method to be valid, it is assumed that the array is located on spatially homogenous, uniform geologic material and thus the spectra, or frequency and amplitude content, of the seismic motions is station independent (*Zerva and Zervas, 2002; Vernon et al., 1991; Hough and Field, 1996*). We do not anticipate that the stations will experience significant site and/or path effects such as large amplifications or focusing effects due to the presence of a large subsurface structure such as a sedimentary basin. However, due to the nature of PBR morphology, it is assumed that the near-surface geology is spatially inhomogenous due to the presence of weathered granite of variable thicknesses at the surface and potentially unexhumed corestones at depth. Thus, the correlation of coherency to refraction microtremor results will provide insight into potential losses of coherency due to inhomogenous subsurface structures. Potential incoherencies could also be better understood with the use of borehole sensors at depth; however, acquiring such data is beyond the scope of this study. Previous studies using widely-spaced arrays have also determined a directional dependency with respect to the epicenter location and fault plane geometry with larger coherency between stations parallel to fault strike (*Claassen, 1985; Der et al., 1984, Abrahamson et al., 1991*). Previous studies have also found a correlation between earthquake magnitude and distance and coherency with lower coherency occurring when there is a large source close to a station (*Somerville et al., 1988; Abrahamson et al., 1991*). However, due to small station spacing these effects are not anticipated to be significant in this study.

Ten seismic stations were installed with short period, weak motion Sercel L22 sensors, RefTek dataloggers, and GPS clocks from IRIS PASSCAL from August 1, 2010 – October 24, 2011 to capture local earthquakes of magnitude 2.5 and greater that occur within 50-100 km of the array (*Figure 3*). The weak motion sensors cover frequency bands from 1 to 100 Hz with a corner frequency of 2 Hz and are set to record 100 samples per second with high gain to amplify the recorded signal (standard convention). Nine of the stations were aligned in a radial array around the PBR with 40-degree separation between stations. A station was also located less than 1 meter from the PBR. Stations were initially located 100 m from the PBR and were moved to 50 meters after 10 months and then 25 meters after an additional 3 months. Instruments were deployed for a total of 15 months from early August 2010 to late October 2011. Analysis of data will be conducted over Spring 2012. Raw seismic data will be converted to SEED (Standard for the Exchange of Earthquake Data) format and data will be analyzed for recorded earthquakes using the SCEC (Southern California Earthquake Center) local earthquake database. Earthquakes will then be selected from the entirety of recorded time, P- and S-wave arrivals will be picked, and coherency calculations will be performed across the stations.

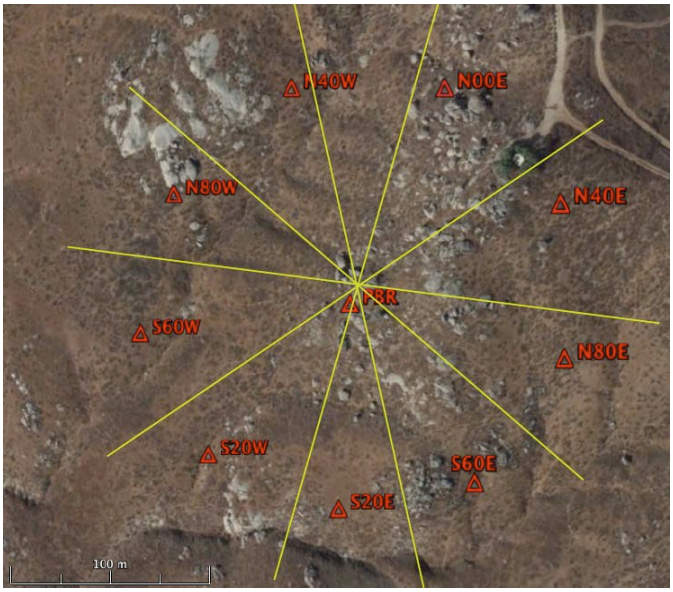


**Figure 5:** Map of 10 seismic stations (red triangles) aligned in radial array with PBR station at the center ReMi linear arrays are represented by yellow lines. (*basemap from USGS, Google Earth*).

## 5. References


Abbott, R.E.; Louie, J.N.; Brune, J.N.; Anooshehpoor, R., " Analysis of Shallow Site Response to LARSE-2 Blasts at Precarious Rock Sites Near the San Andreas Fault," Final Report, 2001.

Abrahamson, N.A.; Schneider, J.F.; Stepp, J.C., "Empirical Spatial Coherency Functions for Application to Soil-Structure Interaction Analyses," *Earthquake Spectra*, Vol. 7, no. 1, 1991.

Anderson, J. G., "Benefits of scenario ground motion maps," *Engineering Geology*, v. 48, 1997, 43-57.

Anooshehpoor, R. and Brune, J.N., " Verification of precarious rock methodology using shake table tests of rock models," *Soil Dynamics and Earthquake Engineering* 22, 917–922, 2002.

Anooshehpoor, A.; Brune, J. N.; Zeng, Y., "Methodology for Obtaining Constraints on Ground Motion from Precariously Balanced Rocks," *Bulletin of the Seismological Society of America*, v. 94, no. 1, 285-303, 2004.

Balco, G.; Stone, J.O.; Lifton, N.A.; Tibor, J.D., "A complete and easily accessible means of calculating surface exposure ages or erosion rates from $^{10}$Be and $^{26}$Al measurements," *Quaternary Geochronology*, vol. 3, 174-195, 2008.

Balco, G.; Purvance, M. D.; Rood, D., "Exposure Dating of Precariously Balanced Rocks," *Quaternary Geochronology (in press)*, 2011.

Bell, J. W.; Brune, J. N.; Liu, T.; Zreda, M.; Yount, J. C., "Dating precariously balanced rocks in seismically active parts of California and Nevada," *Geology*, v. 26, 495-498, 1998.

Boore, D. M., Joyner, W. B., "Site Amplifications for Generic Rock Sites," *Bulletin of the Seismological Society of America*, v. 87, no. 2, 327-341, 1997.

Borcherdt, R. D., "Effects of Local Geology on Ground Motion Near San Francisco Bay," *Bulletin of the Seismological Society of America*, v. 60, no. 1, 29-61, 1970.

Brown, E.T.; Stallard, R.F.; Larsen, M.C.; Raisbeck, G.M.; Yiou, F., "Denudation rates determined from the accumulations of in situ-produced 10Be in the Luquillo Experimental Forest, Puerto Rico," *Earth and Planetary Science Letters*, v. 129, 193-202, 1995.

Brune, J. N., "Precariously Balanced Rocks and Ground-Motion Maps for Southern California," *Bulletin of the Seismological Society of America*, v. 86, no. 1A, 43-54, 1996.

Brune, J. N.; Bell, J. W.; Anooshehpoor, A., “Precariously balanced rocks and seismic risk,” *Endeavour*, v. 20, Issue 4, 168-172, 1996.

Brune, J.N., “Precarious rock evidence for low near-source accelerations for trans-tensional strike-slip earthquakes,” *Physics of the Earth and Planetary Interiors*, v. 137, 229-239, 2003.

Brune, J. N.; Anooshehpoor, A.; Purvance, M. D.; Brune, R. J., “Band of precariously balanced rocks between the Elsinore and San Jacinto, California, fault zones: Constraints on ground motion for large earthquakes,” *Geology*, v. 34, no. 3, 137-140, 2006.

Claassen, J.P., "The estimation of seismic spatial coherence and its application to a regional event," Sandia National Laboratory, SAND85-2093, 1985.

Der., Z.A.; Marshall, M.E.; O'Donnel, A.; McElfresh, T., "Spatial coherence structure and attenuation of the Lg phase, site effects, and the interpretation of the Lg coda," Bulletin of the Seismological Society of America, vol. 74, 1125-1147, 1984.

Dieterich, J.H.; Henyey, T.L.; Mahdyiar, M.; Schwartz, D.; Ward, S.N.; Seismic hazards in southern California: Probable earthquakes, 1994 to 2024, *Bulletin of the Seismological Society of America*, v. 85, 379-439, 1995.

Envicom Corporation, and County of Riverside Planning Department, “Seismic safety and safety elements,” *Technical Report*, Riverside, CA, 1976.

Frankel A.D.; Petersen, M.D.; Mueller, C.S.; Haller, K.M.; Wheeler, R.L.; Leyendecker, E.V.; Wesson, R.L.; Harmsen, S.C.; Cramer, C.H.; Perkins, D.M.; and Rukstales, K.S., " Documentation for the 2002 Update of the National Seismic Hazard Maps," USGS Open File Report 04-420, 2002.

Grant, L.B. and Sieh, K., "Paleoseismic evidence of clustered earthquakes on the San Andreas Fault in the Carrizo Plain, California," *Journal of Geophysical Research*, Vol. 99, no. B4, 6819-6841, 1994.

Haddad, D.E. and Arrowsmith, R., "Assessing the Stability of Precariously Balanced Rocks and their Geomorphic Setting," *Abstract from American Geophysical Union Fall Meeting*, December, 2010.

Hall, D. B., “Modelling failure of natural rock columns,” *Geomorphology*, v. 15, 1996, 123-134.

Holden, E.S., A catalog of earthquakes on the Pacific Coast, 1769-1897, Smithsonian Institution, Washington City, 1898.

Hough, S. E., Field, E. H., "On the Coherence of Ground Motion in the San Fernando Valley," *Bulletin of the Seismological Society of America*, v. 86, no. 6, 1724-1734, 1996.

Louie, J. N., “Faster, better:shear-wave velocity to 100 meters depth from refraction mincrotremor arrays,” *Bulletin of the Seismological Society of America*, v. 91, no. 2, 347-364, 2001.

Maechling, P. J.; Jordan, T. H.; Kesselman, C.; Moore, R.; Minster, J. B.; SCEC Collaboration, "The SCEC Petascale Cyberfacility for Physics-based Seismic Hazard Analysis (PetaSHA): Accelerating SCEC Research Using High Performance Computing," *American Geophysical Union Annual Meeting*, 2007.

Menke, W.; Lerner-Lam, A.L.; Dubendorf, B.; Pacheco, J., "Polarization and Coherence of 5 to 30 Hz Seismic Wave Fields at a Hard Rock Site and Their Relevance to Velocity Heterogeneities in the Crust," *Bulletin of the Seismological Society of America*, v. 80, no. 2, 430-449, 1990.

Nishiizumi, K.; Wintterer, E.; Kohl, C.; Klein, J.; Middleton, R.; Lal, D.; Arnold J., “Cosmogenic ray production rates of 26Al and 10Be in quartz from glacially polished rocks,” Journal of Geophysical Research, v. 94, no. 17, 907-17, 915, 1989.

O'Connell, D.R.H., LaForge, R., Liu, P., "Probabilistic Ground-motion Assessment of Balanced Rocks in the Mojave Desert," *Seismological Research Letters*, v. 78, no. 6, 649-662, 2007.

Okaya, D.; Deelman, E.; Maechling, P.; Wong-Barnum, M.; Jordan, T. H.; Meyers, D.,

"Metadata Management on the SCEC PetaSHA Project: Helping Users Describe, Discover, Understand, and Use Simulation Data in a Large-Scale Scientific Collaboration," American Geophysical Union, Fall Meeting 2007

Petersen,M.D.; Frankel, A.D.; Harmsen, S.C.; Mueller, C.S.; Haller, K.M.; Wheeler,R.L.; Wesson, R.L.; Zeng,Y.; Boyd, O.S.; Perkins, D.M.; Luco, N.; Field, E.H.; Wills, C.J.; Rukstales, K.S., " Documentation for the 2008 Update of the United States National Seismic Hazard Maps, USGS Open File Report 2008-1108, 2008.

Prieto,G.A.; Parker,R.L.; Thomson, D. J.; Vernon, F. L. ; Graham, R.L., " Reducing the bias of multitaper spectrum estimates," *Geophysics Journal International*, 171, 1269–1281, 2007.

Purvance, M.D., "Overturning of slender blocks: numerical investigation and application to precariously balanced rocks in southern California," Ph.D. Thesis, University of Nevada, Reno, Reno, Nevada, 2005.

Purvance, M. D.; Brune, James N.; Abrahamson, Norman A.; Anderson, John G., "Consistency of Precariously Balanced Rocks with Probabilistic Seismic Hazard Estimates in Southern California," *Bulletin of the Seismological Society of America*, v. 98, no. 6, 2629-2640, 2008a.

Purvance, M. D.; Anooshehpoor, Abdolrasool; Brune, James N., "Freestanding block overturning fragilities: Numerical simulation and experimental validation," *Earthquake Engineering and Structural Dynamics*, v. 37, 791-808, 2008b.

Purvance, M.D.; Anooshehpoor, R.; Brune J.N., " Precarious Rock Constraints on Ground Accelerations Associated with Normal Faults," USGS Final Report , Award 07HQGR0028 , 2008c.

Purvance, M.D., Anooshehpoor, A.; Brune, J. N.; "Extreme Ground Motions at Yucca Mountain" *Pacific Earthquake Engineering Research (PEER) Center Final Report*, Fragilities for Precarious Rocks at Yucca Mountain Project, Berkeley, California, 2009.

Schneider, J.F.; Stepp, C.; Abrahamson, N.A., "The spatial variation of earthquake ground motion and effects of local site conditions," *Proceedings 10th World Conference on Earthquake Engineering*, Madrid, Spain, 19-24, 1992.

Shi, B.; Abdolrasool Anooshehpoor, Yuehua Zeng, and James N. Brune, " Rocking and Overturning of Precariously Balanced Rocks by Earthquakes" Bulletin of the Seismological Society of America, Vol. 86, No. 5, pp. 1364-1371, October 1996.

Shaler, N., 1896. Aspects of the Earth. Charles Scribner's Sons, New York.

Steidl, J. H., Tumarkin, A. G., Archuleta, R. J., "What is a Reference Site?," *Bulletin of the Seismological Society of America*, v. 86, no. 6, 1733-1748, 1996.

Stirling, M. W.; Anooshehpoor, A. ; Brune, J. N.; Biasi, G. P.; Wesnousky, Steven G., "Assessment of the Site Conditions of Precariously Balanced Rocks in the Mojave Desert, Southern California," *Bulletin of the Seismological Society of America*, v. 92, no. 6, 2139-2144, 2002.

Stirling, M.; Ledgerwood, J.; Liu, T.; Apted, M., " Age of Unstable Bedrock Landforms Southwest of Yucca Mountain, Nevada, and Implications for Past Ground Motions," *Bulletin of the Seismological Society of America*, Vol. 100, No. 1, pp. 74–86, February 2010.

Thomson, D. J., "Spectrum estimation and harmonic analysis," *Proc. IEEE*, 70, 1055- 1096, 1982.

Tucker, B.E.; King J.L.; Hatzfeld, D.; Nersesov, I.L.; "Observations of Hard Rock Site Effects," *Bulletin of the Seismological Society of America*, v. 74, no. 1, 121-136, 1984.

Twidale, C.R., *Analysis of Landforms*, John Wiley & Sons Australasia Pty Ltd, Sydney, 1976.

Vernon, F.; Fletcher, J.; Carrol, L; Chave, A.; Sembera, E., " Coherence of Seismic Body Waves From Local Events as Measured by a Small-Aperture Array" *Journal of Geophysical Research*, VOL. 96, NO. B7, 11,981-11,996, 1991.

Walker, M., *Quaternary Dating Methods*, John Wiley & Sons, Ltd, England, 2005.
Wood, H. D., "Preliminary report on the Long Beach earthquake", *Bull. Seism. Soc. Am.* 23, 42–56, 1933.
Yim, C.S.; Chopra, A.; Penzin, J., “Rocking response of rigid blocks to earthquakes,” *Earthquake Engineering and Structural Dynamics*, v. 8, 565-587, 1980.
Zembaty, Z. and Krenk, S., "Spatial Seismic Expectations and Response Spectra," *Journal of Engineering Mechanics,* Vol. 119, No. 12,1993.
Zerva, A. and Zervas, V., "Spatial Variation of Seismic Ground Motions: An overview," *Appl Mech Rev* vol 55, no 3, 2002.